arXiv:1804.03951v2 [q-bio.PE] 31 Oct 2018

Complex pattern formation driven by the interaction of stable fronts in a competition-diffusion system

Lorenzo Contento* Masayasu Mimura †

February 22, 2022

The ecological invasion problem in which a weaker exotic species invades an ecosystem inhabited by two strongly competing native species is modelled by a three-species competition-diffusion system. It is known that for a certain range of parameter values competitor-mediated coexistence occurs and complex spatio-temporal patterns are observed in two spatial dimensions. In this paper we uncover the mechanism which generates such patterns. Under some assumptions on the parameters the three-species competition-diffusion system admits two planarly stable travelling waves. Their interaction in one spatial dimension may result in either reflection or merging into a single homoclinic wave, depending on the strength of the invading species. This transition can be understood by studying the bifurcation structure of the homoclinic wave. In particular, a time-periodic homoclinic wave (breathing wave) is born from a Hopf bifurcation and its unstable branch acts as a separator between the reflection and merging regimes. The same transition occurs in two spatial dimensions: the stable regular spiral associated to the homoclinic wave destabilizes, giving rise first to an oscillating breathing spiral and then breaking up producing a dynamic pattern characterized by many spiral cores. We find that these complex patterns are generated by the interaction of two planarly stable travelling waves, in contrast with many other well known cases of pattern formation where planar instability plays a central role.

Keywords competition-diffusion system · ecological invasion · competitor-mediated coexistence · travelling wave · pattern formation · travelling breather

Mathematics Subject Classification 35Q92 · 92D25 · 35K57 · 35C07 · 35B36

*Meiji Institute for Advanced Study of Mathematical Sciences, Meiji University, Tōkyō 164-8525, Japan
✉ lorenzo.contento@gmail.com ORCID: orcid.org/0000-0002-7901-2172
†Department of Mathematical Engineering, Musashino University, Tōkyō 135-8181, Japan

1 An introduction to competitor-mediated coexistence in the three-species competition-diffusion system

Investigation of the origin of the rich species biodiversity observed in nature has been an important and long-standing endeavour in theoretical ecology. Since Gause's pioneering work on bacterial cultures in the 1930s [27], one of the foundations of this field has been the *competitive-exclusion principle*: two or more species which are competing for the same limited resources cannot coexist if the environmental factors are constant in space and time. While in many cases species biodiversity in actual ecosystems is indeed linked to a changing environment or to niche specialization, there are some examples where a high number of coexisting species is observed even if resources are scarce and the environmental factors constant (e.g., Hutchinson's well-known paradox of the plankton [41]). In order to reconcile such an apparent contradiction with the competitive-exclusion principle, many different mechanisms have been proposed. Of particular theoretical interest are those that rely only on indirect competition dynamics to enable coexistence, such as *competitor-mediated coexistence*, where the presence of a third competitor allows two competing species to coexist, even if they are unable to do so otherwise.

In order to understand competitor-mediated coexistence from a mathematical point of view, we consider an ecosystem inhabited by three species, two of which are competing species native to the ecosystem and the other is an exotic competing species invading from the outside. This situation can be described by the following *three-species competition-diffusion system* of Lotka-Volterra type (see, e.g., [22, 2]):

$$\begin{cases} u_t = d_1\,\Delta u \; + (r_1 - u \; - b_{12}\,v - b_{13}\,w)\,u, \\ v_t = d_2\,\Delta v \; + (r_2 - v \; - b_{21}\,u - b_{23}\,w)\,v, \\ w_t = d_3\,\Delta w + (r_3 - w - b_{31}\,u - b_{32}\,v\,)\,w, \end{cases} \tag{CD}$$

where $u(x,t)$, $v(x,t)$ and $w(x,t)$ are the population densities of the three competing species at the spatial position x and time t. We will take w to be the density of the exotic species and in the following, with slight abuse of notation, we will denote by u, v, w both the three competing species and their densities. The positive parameters d_i, r_i and b_{ij}, with $i, j = 1, 2, 3$ and $i \neq j$, denote the diffusion rates, the intrinsic growth rates and the inter-specific competition rates, respectively. All of them are constant in time and space, since we want to investigate the effects of indirect competition in a homogeneous environment. In this paper we are mainly interested in the patterns displayed by the solutions of the initial value problem (P) for the system (CD) on a bounded and convex spatial domain $\Omega \subset \mathbb{R}^2$. The initial conditions are

$$u(x,0) = u_0(x), \quad v(x,0) = v_0(x), \quad w(x,0) = w_0(x), \quad \text{for all } x \in \Omega, \tag{IC}$$

where $u_0(x)$, $v_0(x)$ and $w_0(x)$ are given non-negative functions, and zero-flux boundary conditions are imposed on $\partial\Omega$, i.e.,

$$\partial_{\boldsymbol{n}} u = \partial_{\boldsymbol{n}} v = \partial_{\boldsymbol{n}} w = 0, \quad \text{on } \partial\Omega \times (0,\infty)\,, \tag{BC}$$

where $\partial_{\boldsymbol{n}}$ denotes the derivative along the direction normal to the boundary $\partial\Omega$. Such boundary conditions mean that immigration/emigration is not possible.

In this paper, we consider the invading species w to be "weaker" than u and v in their habitat. This is the ecologically plausible situation since the native species have evolved there while the exotic one originated in a different ecosystem. Thus, we first need to study what it means for a

species to be weaker or stronger than another. We start by considering the relative competitive strength of any couple of species when they are taken in absence of the third one. We will use (u, v) as our example, but the same also holds for (v, w) and (w, u). In absence of the exotic species w, i.e., for $w \equiv 0$, the system (CD) reduces to the two-species competition-diffusion system for u and v given by

$$\begin{cases} u_t = d_1 \Delta u + (r_1 - u - b_{12}\, v)\, u, \\ v_t = d_2 \Delta v + (r_2 - v - b_{21}\, u)\, v. \end{cases} \tag{1}$$

First, we study what happens if the species are not able to move, i.e., if we set $d_1 = d_2 = 0$ in (1). The resulting system of ordinary differential equations is the well-known Lotka-Volterra competition system (see, e.g., [58]). It admits three equilibria: $(0, 0)$, where both species are absent; $(r_1, 0)$, where the first species is alone at its carrying capacity; $(0, r_2)$, where the second species is alone at its carrying capacity; and (u^*, v^*), a coexistence equilibrium which is admissible from a modelling point of view only when $u^*, v^* \geq 0$. The equilibrium $(0, 0)$ is always unstable, while the stability of the others depends on the parameter values. Denoting by $\rho = r_2/r_1$ the relative growth rate of the two species and by $\tilde{b}_{12} = \rho b_{12}$ and $\tilde{b}_{21} = b_{21}/\rho$ the non-dimensionalized competition rates, four situations can be distinguished:

(i) $\tilde{b}_{12} < 1$ and $\tilde{b}_{21} > 1$. Then, $(r_1, 0)$ is stable, $(0, r_2)$ is unstable and (u^*, v^*) is not admissible. Orbits starting from non-negative initial conditions will in general converge to $(r_1, 0)$ as time tends to infinity. Since the species u always drives v to extinction, in this case we say that u is *absolutely stronger* than v.

(ii) $\tilde{b}_{12} > 1$ and $\tilde{b}_{21} < 1$. Then, $(r_1, 0)$ is unstable, $(0, r_2)$ is stable and (u^*, v^*) is not admissible. Similarly to the previous point, v is absolutely stronger than u.

(iii) $\tilde{b}_{12} < 1$ and $\tilde{b}_{21} < 1$. Then, $(r_1, 0)$ and $(0, r_2)$ are unstable, while (u^*, v^*) is admissible and stable. Orbits starting from non-negative initial conditions will in general converge to (u^*, v^*), leading to the coexistence of the species u and v. Such a case is called *weak competition*. At first sight it looks like a violation of the competitive exclusion principle, but this situation is generally associated to the existence of extra resources which are not the object of competition. For this reason, this case will not be further considered in this paper.

(iv) $\tilde{b}_{12} > 1$ and $\tilde{b}_{21} > 1$. Then, $(r_1, 0)$ and $(0, r_2)$ are stable, while (u^*, v^*) is admissible and unstable. Orbits will converge to either $(r_1, 0)$ or $(0, r_2)$, depending on the particular choice of non-negative initial conditions. In this case we say that the species are *strongly competing*. Coexistence is impossible but there is no clearly dominant species as in the first two cases.

Now we consider the case in which the species can disperse randomly, i.e., $d_1, d_2 > 0$ in (1). We suppose that the domain $\Omega \subset \mathbb{R}^2$ is convex and bounded and we impose appropriate initial and boundary conditions analogous to (IC) and (BC). If u is absolutely stronger than v, then all positive solutions $(u, v)(x, t)$ of the initial value problem will converge to the spatially-homogeneous equilibrium $(r_1, 0)$. If u and v are strongly competing instead, the spatially-homogeneous equilibria $(r_1, 0)$ and $(0, r_2)$ are both stable and any positive solution generically converges to one of them [39, 47]. This means that competitive exclusion occurs

between the two species u and v. We remark that if Ω is not convex this is no longer true and the species may coexist by spatial segregation [53].

Given this result, in the case of strong competition it is natural to wonder whether it is possible to determine which one of the two species will be dominant in the long run. As we have already remarked, in the absence of diffusion either species may survive, which one depending on the initial density values. Thus, in presence of diffusion too, the surviving species must depend on the initial conditions. However, let us suppose that at the initial time the two species are segregated, in the sense that the domain can be partitioned in two (not necessarily connected) regions, in one of which the species u is alone at its carrying capacity while in the other v is alone at its carrying capacity. For these quite general and reasonable initial conditions, the dominant species in the long run can be determined from the sign of the velocity of the interface between the two regions, which can be obtained by studying a one-dimensional travelling wave problem for (1). We recall that a travelling wave solution is a solution whose spatial profile moves at a constant velocity without changing shape. It has the form $(u, v)(x, t) = (U, V)(x - c\,t)$ for all $x \in \mathbb{R}$ and all $t \in \mathbb{R}$, where c is the travelling wave velocity and $(U, V)(z)$ is the travelling wave profile. In the case of the one-dimensional travelling waves of (1), the profile and the velocity must satisfy

$$\begin{cases} d_1\, U_{zz} + c\, U_z + (r_1 - U - b_{12}\, V)\, U = 0, \\ d_2\, V_{zz} + c\, V_z + (r_2 - V - b_{21}\, U)\, V = 0, \end{cases} \tag{2}$$

on the whole real line. This system of elliptic equations is also known as the *travelling wave equation*. Usually, additional boundary conditions are imposed at $z = \pm\infty$ in order to specify the asymptotic behaviour of the wave far from the front region. Since we are interested in the motion of the interface between the region where u is dominant and the region where v is dominant, we will look for travelling waves of (1) satisfying the asymptotic boundary conditions

$$\begin{aligned} \lim_{z \to -\infty} (U, V)(z) &= (r_1, 0), \\ \lim_{z \to +\infty} (U, V)(z) &= (0, r_2). \end{aligned} \tag{3}$$

In the case of strong competition, there exists a non-negative and bounded travelling wave solution of (1) with boundary conditions (3) and velocity $c = c_{uv}$ which is unique (up to translations) and stable [45, 46]. Then, the sign of c_{uv} determines the direction of the motion of the interface between the species u and v. If for example $c_{uv} > 0$, then the interface moves to the right, resulting in the species v being completely replaced by u everywhere as $t \to \infty$ in the one-dimensional travelling wave solution. In such a case we expect that, for initial conditions where the two species are segregated and even in higher spatial dimensions, the species u will always be the one to survive in the long run. For this reason, if $c_{uv} > 0$ we say that u is *stronger in space* than v. Conversely, if $c_{uv} < 0$, then v is stronger in space than u.

Remark 1. In this paper the order of the subscripts in a travelling wave velocity reflects the boundary conditions at the spatial infinities. For example, in contrast with the symbol c_{uv} introduced in the above paragraph, the symbol c_{vu} denotes the velocity of a wave whose profile tends to the state where v is alone at carrying capacity as $z \to -\infty$ and to the state where u is alone at carrying capacity as $z \to \infty$. By the uniqueness property discussed above, the profile of this wave coincides with that of the wave with velocity c_{uv} (up to a reflection with respect to the origin and a translation) and we have that $c_{vu} = -c_{uv}$.

If the species u is absolutely stronger than v instead, intuitively we expect that u is also stronger in space. In this case, the equilibrium $(0, r_2)$, which appears in the boundary conditions

(3), is unstable. Then, it seems reasonable that the interface always moves in the direction from the stable equilibrium to the unstable one, since at any point in space the solution tends to the stable state. In [44] it was shown that problem (2) and (3) admits a continuum of solutions, meaning that the travelling wave is not unique. In particular, there exists a minimal propagation speed $\bar{c} > 0$ such that problem (2) and (3) admits a solution for any choice of $c \geq \bar{c}$. This situation is analogous to the Fisher-KPP equation, which is also monostable. As a consequence, all travelling waves have positive velocity so that the species u always drives the species v to extinction and u is stronger in space than v. Similarly, if v is absolutely stronger than u then it is also stronger in space.

In the rest of this paper, we will make the following assumptions on the two native species u and v:

(i) u and v are strongly competing, i.e.,

$$\frac{r_2}{r_1} b_{12} > 1 \quad \text{and} \quad \frac{r_1}{r_2} b_{21} > 1; \tag{A1}$$

(ii) u is stronger in space than v, i.e.,

$$c_{uv} > 0. \tag{A2}$$

For example, if $d_1 = d_2$, $r_1 = r_2$ and $1 < b_{12} < b_{21}$ are taken, then clearly both (A1) and (A2) hold.

Going back to the three-species cases, we take r_3 as a free parameter and investigate whether competitor-mediated coexistence occurs when the exotic species w invades the ecosystem inhabited by the native species u and v. Since r_3 is the intrinsic growth rate of w, its value reflects the suitability of the new environment for the invader w and thus its strength relative to the native species. Then, this parameter can be expected to play a fundamental role in the dynamics after the invasion.

First, we consider two extreme situations for the value of r_3. When r_3 is sufficiently large compared with the other parameters, the exotic species w is absolutely stronger than both native species u and v. In particular, in the ordinary differential equation obtained in absence of diffusion the equilibrium $(0, 0, r_3)$ is stable, while the equilibria $(r_1, 0, 0)$ and $(0, r_2, 0)$ are unstable. In this case numerical simulations show that any positive solution $(u, v, w)(t)$ of (P) tends to $(0, 0, r_3)$, which means that the exotic species is always able to invade the new ecosystem, driving the native species to extinction. On the other hand, when r_3 is sufficiently small, the invader w is absolutely weaker than both u and v and the equilibria $(r_1, 0, 0)$ and $(0, r_2, 0)$ are stable, while $(0, 0, r_3)$ is unstable. In this case, the numerical solutions tend to either $(r_1, 0, 0)$ or $(0, r_2, 0)$, that is, the invasion is never successful, the invading species w dies out and the situation is reduced to the two-species case. In our case in particular, thanks to assumptions (A1) and (A2), the final state is $(r_1, 0, 0)$ for general initial conditions. We remark that in the limiting situations where r_3 is either very large or very small, the same results can also be proven analytically [11].

Since competitor-mediated coexistence never occurs for extreme values of r_3, we should consider the case where r_3 is neither large nor small and the exotic species w is of comparable strength with respect to at least one of the native species. A first possibility is to suppose that the invader w is strongly competing with both native species u and v. Then, in absence of diffusion the equilibria $(r_1, 0, 0)$, $(0, r_2, 0)$ and $(0, 0, r_3)$ are all stable. Moreover, we find that there exists a unique travelling wave solution connecting $(0, r_2, 0)$ on the left to $(0, 0, r_3)$ on the

right, having velocity c_{vw} and for which $u \equiv 0$. Similarly, there exists a unique travelling wave solution connecting $(0, 0, r_3)$ on the left to $(r_1, 0, 0)$ on the right, having velocity c_{wu} and for which $v \equiv 0$. Then, if the parameters are chosen so that $c_{uv}, c_{vw}, c_{wu} > 0$, we say that (CD) possesses the *cyclic ordering property* on competition in space. This means that u invades v, v invades w and w invades u. Thanks to this rock-paper-scissors-like relationship among u, v and w, one can expect that the three species may be able to coexist, exhibiting a dynamic structure of rotating spiral patterns in space. This situation is discussed more precisely in [22]. Instead of considering strongly competing species, each species may be taken to be absolutely stronger than the next, from which cyclic competition follows immediately [2].

In this paper we are concerned with the ecologically realistic case of an invading species w weaker than the native species u and v. Thus, the setting described above is not the correct one. As a more realistic situation, we assume that w is absolutely weaker than v but strongly competing (not absolutely stronger) with u. The former holds if

$$\frac{r_2}{r_3}\, b_{32} > 1 > \frac{r_3}{r_2}\, b_{23}, \tag{A3}$$

while the latter holds if

$$\frac{r_1}{r_3}\, b_{31} > 1 \quad \text{and} \quad \frac{r_3}{r_1}\, b_{13} > 1. \tag{A4}$$

Under (A1), (A3) and (A4), in the diffusion-free system associated to (CD) the equilibria $(r_1, 0, 0)$ and $(0, r_2, 0)$ are locally stable, while $(0, 0, r_3)$ is saddle-type unstable.

Since we want to focus on coexistence originating from the interplay of competition dynamics and diffusion, we need to ensure that coexistence is not possible in the trivial case when diffusion is absent. This is done by imposing the following additional assumption:

$$\text{In the diffusion-free system associated to (CD), the positive coexistence equilibrium either does not exist or is saddle-type unstable.} \tag{A5}$$

Then, under assumptions (A1) and (A3–5), positive solutions $(u, v, w)(t)$ of the diffusion-free system associated to (CD) tend in general to either $(r_1, 0, 0)$ or $(0, r_2, 0)$ [40, 67].

From this result, it seems reasonable to expect that competitor-mediated coexistence never occurs even when the species can move randomly in space. Indeed, this is the case if all the diffusion rates d_i $(i = 1, 2, 3)$ are very large [17], that is, all orbits of (P) converge to one of the two spatially-homogeneous equilibria $(r_1, 0, 0)$ and $(0, r_2, 0)$. However, we will show that this is no longer the case if the diffusion rates d_i are sufficiently small and that it is possible for u, v and w to coexist even if the invader w is weaker, i.e., cannot survive, in the diffusion-free system. In order to do that, we set the parameter values in (CD) as

$$\begin{aligned} &d_1 = d_2 = d_3 = 1, \\ &r_1 = r_2 = 28, \\ &b_{12} = 22/21, \quad b_{13} = 4, \\ &b_{21} = 1.87, \quad\ \ b_{23} = 3/4, \\ &b_{31} = 26/21, \quad b_{32} = 22/21, \end{aligned} \tag{4}$$

and take r_3 as a free parameter [56, 10]. It can be shown that, as long as $r_3 \in (7, 29 + 1/3)$, the assumptions (A1–5) are satisfied.

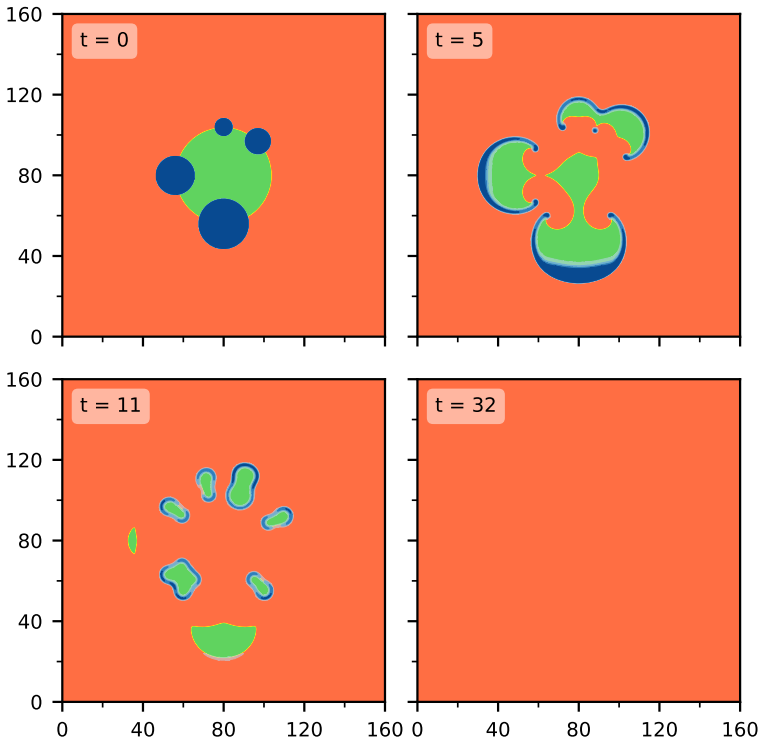


Figure 1 Invasion by the exotic species w when $r_3 = 26.55$. Areas where $u > v$ (respectively, $v > u$) are plotted in red (respectively, green) and the interface between the two is highlighted in yellow. On top of this layer w has been superimposed in blue colour, the darker the higher its density. More details can be observed by zooming in in the electronic version.

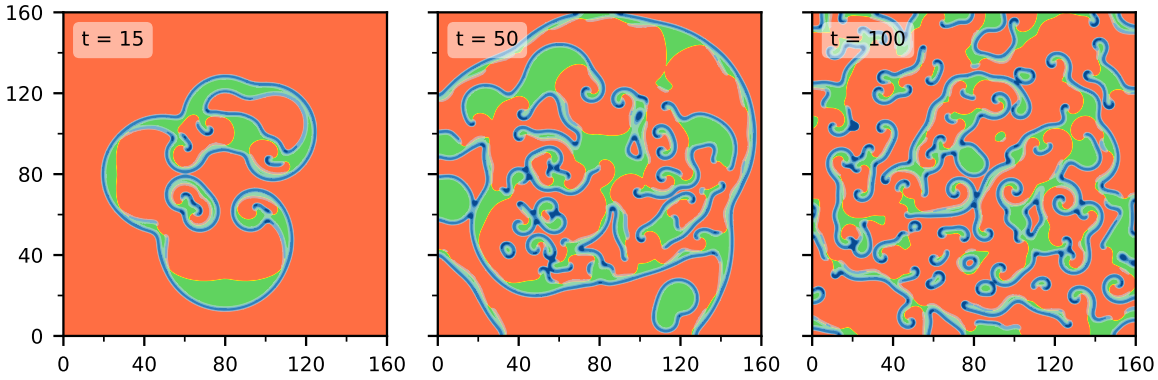


Figure 2 Invasion by the exotic species w when $r_3 = 26.75$. Initial conditions are the same as in Figure 1.

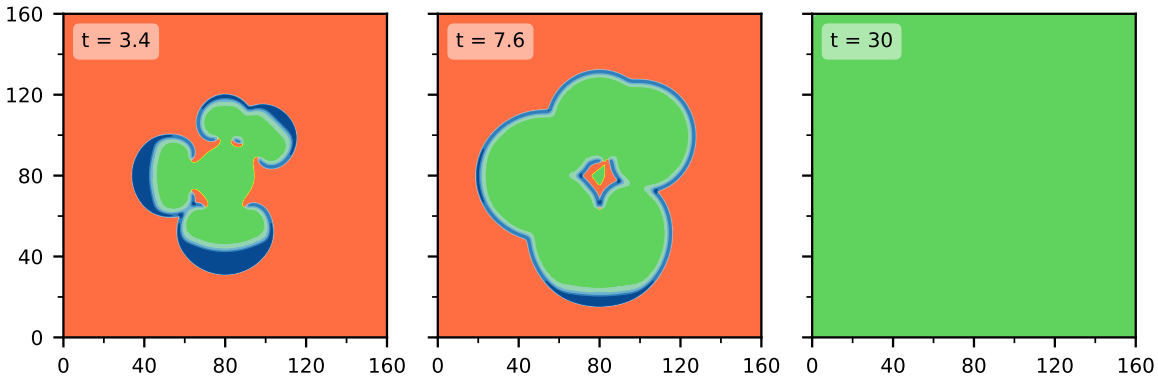


Figure 3 Invasion by the exotic species w when $r_3 = 28$. Initial conditions are the same as in Figure 1.

We consider a square domain Ω and the initial conditions shown in the first panel of Figure 1, where the exotic species w (in blue colour) invades near the interface between the native species u and v (in red and green colour, respectively). In absence of w the region inhabited by v would shrink by competitive exclusion and u would eventually occupy the whole domain Ω. This is still true even with the addition of w when r_3 is relatively small, as shown in Figure 1 for $r_3 = 26.55$. On the other hand, when r_3 is relatively large, the species v will be the only one surviving at the end, as can be seen in Figure 3 for $r_3 = 28$. Note that also in this case competitive exclusion occurs, but the final outcome differs from the one in Figure 1: thanks to the presence of the invading species w and cyclic competition, v is able to replace u as the dominant species in the long run. Finally, when r_3 has a suitable intermediate value, a complex spatio-temporal pattern appears and competitor-mediated coexistence can be observed, as shown in Figure 2 for $r_3 = 26.75$. Animations for the simulations in Figures 1, 2 and 3 can be found at [15].

From the simulation results shown in Figures 1, 2 and 3, it is clear that the patterns produced by the the three-species competition-diffusion system (CD) depend sensitively on the value of r_3. From a mathematical point of view, the understanding of the nature of this dependence, and in particular determining the conditions for which competitor-mediated coexistence occurs, is a problem of great interest.

We should note that complex spatio-temporal patterns such as labyrinthine patterns, spot replications and spiral turbulence have been already observed in other reaction-diffusion systems. The mechanisms generating such patterns are diverse and have been intensively studied from both experimental and analytical viewpoints. Given the wealth of examples in the literature we will just give a far from exhaustive list and mention only some of the most relevant results.

As can be seen in Figure 2, spiral cores appear to be an important feature of the patterns displayed by our three-species competition-diffusion system. Regular and stable spirals often appear in excitable and oscillatory systems, such as the FitzHugh-Nagumo system, in correspondence to a stable travelling pulse. As parameters are varied, such spirals may destabilize (either near the core or far away from it). Then, the spiral often breaks up leading to complex spatio-temporal patterns (*spiral turbulence*, e.g., [69, 3, 66]) resembling those in Figure 2. More in general, instabilities are often capable of generating complex patterns. For example, we refer to [55] for the case of an unstable expanding ring in a bistable reaction-diffusion system and to

[62, 50] for spot instabilities in autocatalytic reaction-diffusion systems.

As we will see in the following, another feature of the patterns shown in Figures 1, 2 and 3 is that they can be thought as being generated from the interaction of two stable counter-propagating fronts. Also in bistable FitzHugh-Nagumo-like systems, depending on the parameter values, it is possible to observe a similar couple of stable counter-propagating fronts, which are generated from a pitchfork bifurcation often referred to as the nonequilibrium Ising-Bloch (NIB) bifurcation (see, e.g., [34, 33]). These two fronts can form regular spirals and these spirals can destabilize by planar instability, again generating complex patterns of various shapes [32]. The behaviour of such fronts in response to curvature perturbations and the consequent spiral nucleation has been studied in [24, 37, 36]. NIB bifurcations and the associated patterns have also been observed experimentally in several settings, such as parametrically-forced oscillating systems [18, 19, 23, 52, 4, 30], bistable chemical reactions [38], liquid crystals [54, 26] and non-linear optical systems [61, 25, 64].

Keeping these earlier studies in mind, we will shed light on the mechanism behind the complex dynamical pattern of Figure 2. Our approach will be to first study the one-dimensional case, in particular travelling waves and their interaction, and then use the insight so obtained to explain the two-dimensional case.

2 One-dimensional travelling wave solutions

Since the species v is absolutely stronger than w by (A3), we know that $c_{vw} > 0$, where c_{vw} is the non-unique velocity of the travelling wave solutions connecting $(0, r_2, 0)$ and $(0, 0, r_3)$ [44]. Since the species w and u are strongly competing by (A4) instead, there exists a unique travelling wave solution connecting $(0, 0, r_3)$ and $(r_1, 0, 0)$ with velocity c_{wu} [45, 46]. We will assume that

$$c_{wu} > 0, \tag{A6}$$

which is satisfied for the parameter choices given in (4).

Assumptions (A2), (A3) and (A6) imply that (CD) possesses the cyclic ordering property on competition in space. Then, we may expect species coexistence to occur, similarly to [22, 2] where the same ordering property applies. This is indeed the case, as we have shown at the end of the previous section. In particular, by looking closely at Figures 2 and 3, we see that Ω is essentially partitioned in two regions: one where the species u is dominant and $(u, v, w) \approx (r_1, 0, 0)$ and the other where v is dominant instead and $(u, v, w) \approx (0, r_2, 0)$. If, somehow arbitrarily, we define these two regions as the ones where $u > v$ and $v < u$ respectively, then the interface between them is given by the line where $u = v$. By examining again the simulation results, we see that this interface can be classified into two kinds. The first one is observed in the absence of the invader w (yellow interfaces in the figures) and moves in the direction from u towards v. This interface is the two-dimensional analogous of the one-dimensional travelling wave connecting $(r_1, 0)$ and $(0, r_2)$ in the two-species competition-diffusion system (1). On the other hand, the second kind of interface is characterized by the presence of the invading species w near the front (blue interfaces in the figures). Such interfaces move in the direction from v towards u and result in the usually weaker species v displacing the usually stronger species u, reversing the "natural" strength relationship occurring in absence of w. This is possible thanks to the cyclic competition in space, which allows for w to initially replace u and for v to replace w immediately after. Moreover, it suggests that there exists a travelling wave solution connecting $(r_1, 0, 0)$ and $(0, r_2, 0)$ in which all species are present.

Under our assumptions, equilibria $(r_1, 0, 0)$ and $(0, r_2, 0)$ are stable in the system of ordinary differential equations obtained from (CD) in absence of diffusion. Now we discuss the existence of travelling wave solutions of (CD) connecting these two equilibria. The profile $(U, V, W)(z)$ and velocity c of such a travelling wave must satisfy the travelling wave equation

$$\begin{cases} d_1 U_{zz} + c U_z + (r_1 - U - b_{12} V - b_{13} W) U = 0, \\ d_2 V_{zz} + c V_z + (r_2 - V - b_{21} U - b_{23} W) V = 0, \\ d_3 W_{zz} + c W_z + (r_3 - W - b_{31} U - b_{32} V) W = 0, \end{cases} \tag{5}$$

with the asymptotic boundary conditions

$$\begin{aligned} \lim_{z \to -\infty} (U, V, W)(z) &= (r_1, 0, 0), \\ \lim_{z \to +\infty} (U, V, W)(z) &= (0, r_2, 0). \end{aligned} \tag{6}$$

Clearly the unique solution of the two-species travelling wave problem given by (2) and (3) can be extended to a solution of problem (5) and (6) by setting $W \equiv 0$. We call such a solution the *trivial* travelling wave solution of (CD). Its velocity $c_{uv} > 0$ and its profile $(U, V)(z)$ are independent of the free parameter r_3. Moreover, if r_3 is relatively small, the trivial travelling wave is stable in the full three-species system [21]. For the choice of parameters given in (4), we have $c_{uv} \approx 2.575$ and the wave profile is shown in Figure 5 (top-left panel).

Does the problem (5) and (6) admit *non-trivial* solutions in which $W(z)$ is not zero everywhere? Recently, it has been shown that non-trivial solutions never exist if r_3 is sufficiently small [9]. On the other hand, there are only a few analytical results on the existence of non-trivial solutions [8]. Numerically, the difficulty lies in finding the right parameter values for which non-trivial solutions exists. Guided by our ecologically motivated assumptions and the values obtained in [8], we have obtained the values shown in (4). For such a choice of parameters, we have used the numerical continuation software AUTO [20] to compute the global structure of the non-trivial solutions of (5) and (6) as the free parameter r_3 is varied. In Figure 4 we have plotted the resulting bifurcation diagram for both trivial and non-trivial solutions of (5) and (6).

When r_3 is small there is no non-trivial travelling wave solution. However, as r_3 increases, two non-trivial travelling waves appear from a saddle-node bifurcation at $r_3 = r_F \approx 26.674$. One of them (the lower branch) is stable with velocity c_{uvw}, while the other (the upper branch) is unstable with velocity $\tilde{c}_{uvw}$. The unstable branch eventually connects to the trivial travelling wave branch at a *drift bifurcation* point.

A drift bifurcation of a travelling wave occurs when its zero eigenvalue is no longer simple. A stable travelling wave has no eigenvalues with positive real part and a simple zero eigenvalue. This zero eigenvalue and the associated eigenfunction (Goldstone mode G, given by the derivative of the profile with respect to the space variable) are linked to the invariance of the traveling wave with respect to translations: a small perturbation proportional to the Goldstone mode will result in a shifted profile which continues to move with the same shape and velocity. However, as the parameters change, an eigenvalue with zero imaginary part may cross the imaginary axis. Then, for a specific choice of the parameters we have that zero is no longer a simple eigenvalue. If it is also no longer regular, we say that a drift bifurcation has occurred. Then, in addition to the Goldstone mode, there exists a generalized eigenfunction (propagator mode P) which causes the traveling wave to destabilize. In order to understand what happens to the destabilized wave, let us consider how a small perturbation $\psi(t)$ to the wave profile evolves with time t.

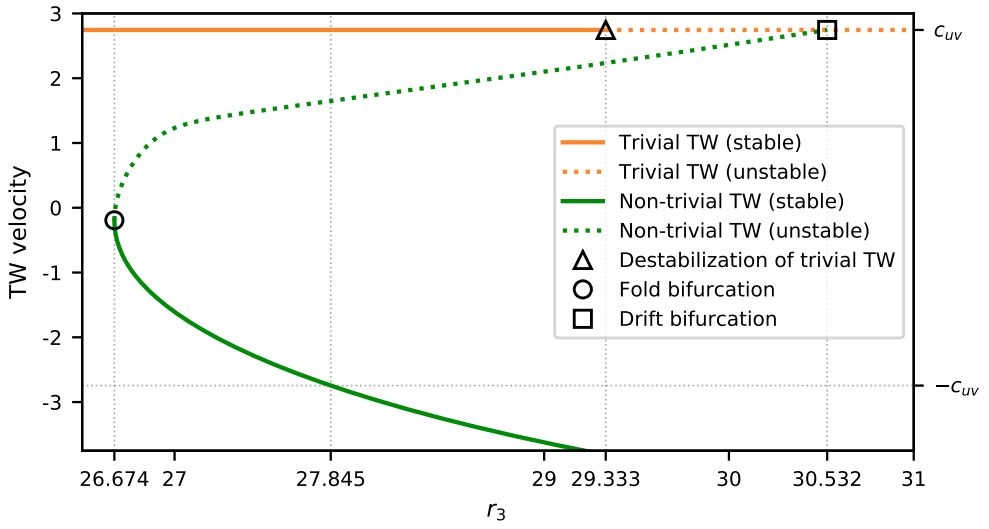


Figure 4 Bifurcation diagram for the trivial and non-trivial one-dimensional travelling wave solutions of (CD). The travelling wave velocity is plotted as a function of the free parameter r_3.

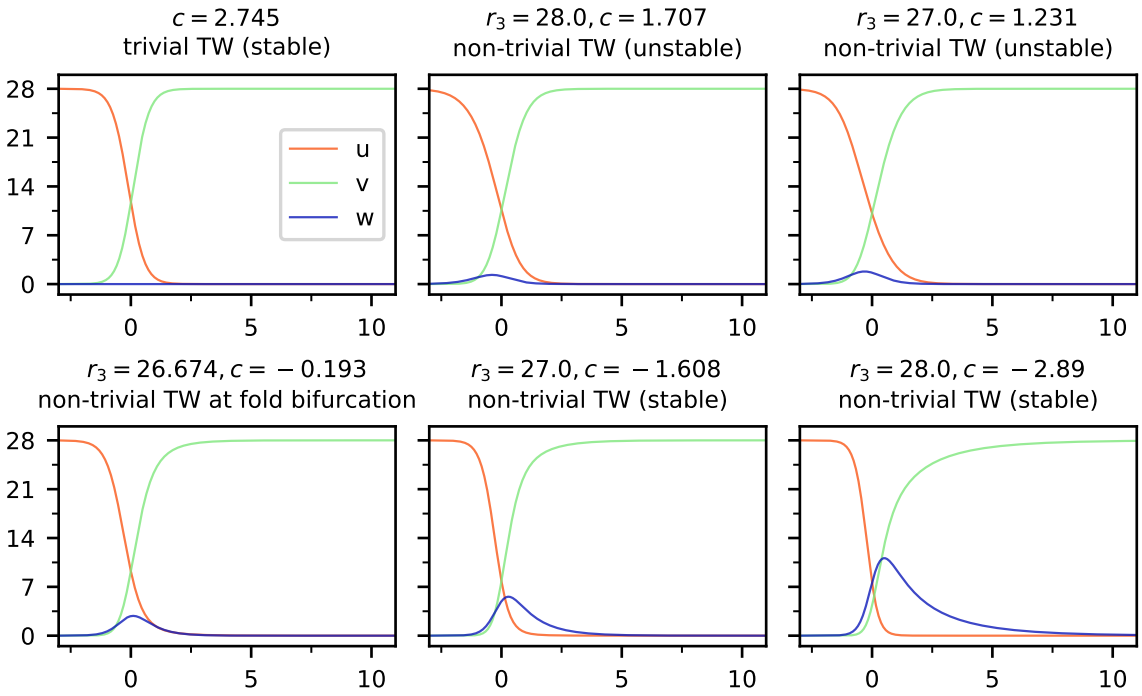


Figure 5 Profiles of the trivial and non-trivial one-dimensional travelling wave solutions of (CD) for different values of the free parameter r_3.

The function ψ satisfies the evolution equation given by $\psi_t = \mathcal{L}\psi$, where the linear operator $\mathcal{L}$ is obtained by linearizing the travelling wave equation around the travelling wave profile. The Goldstone and propagator modes satisfy $\mathcal{L}G = 0$ and $\mathcal{L}P = G$ by definition. Supposing that the initial perturbation is proportional to the propagator mode, i.e., $\psi(0) \propto P$, we obtain that $\psi(t) \propto P + tG$. Since an infinitesimal perturbation in the Goldstone mode is equivalent to shifting the wave profile, the perturbed solution propagates with constant velocity in the reference frame of the original wave: a new travelling wave, with a different profile and velocity, has been generated from the drift bifurcation. For more details about drift bifurcations see, e.g., [6, 31]. The existence of a drift bifurcation point on the trivial travelling wave branch (with r_3 as the free parameter) of a three-species competition-diffusion system has been recently discussed in [21].

Our case is slightly different from the simplest case presented above (and also from [21]), where the original travelling wave loses stability at the drift bifurcation point while the generated branch is stable. Here instead, as can be seen in Figure 4, the trivial wave has already lost stability by the time it reaches the drift bifurcation point: when r_3 crosses the threshold $29 + 1/3$, the species v and w become weakly competing and the equilibrium $(0, r_2, 0)$ loses stability in the diffusion-free system. The same discussion as above apply, with the caveat that the new travelling wave branches generated at the drift bifurcation are all unstable. Finally, we remark that while in Figure 4 we have plotted the non-trivial travelling wave branch only up to the drift bifurcation point, this branch continues beyond it, as can be expected from such a bifurcation. However, the associated travelling wave solutions are no longer admissible from a modelling point of view since the density of w around the front becomes negative.

In Figure 5 we show the evolution of the profile of the non-trivial travelling wave along its solution branch. We start from the drift bifurcation point, where a small peak of the invading species w appears near the interface between the native species u and v, marking the origin of the non-trivial wave from the trivial one. As we follow the branch, the peak gradually grows in size and at the same time the velocity of the wave decreases, until it becomes negative and the direction of wave propagation is inverted. This is reasonable from a modelling point of view, since by the cyclic competition property the presence of the invader w is harmful to u and beneficial to v. Thus, the speed of an interface between u and v is controlled by the density of w around it.

We are also interested in seeing what happens if we perturb the trivial travelling wave by increasing the density of w near the interface. For relatively small values of r_3, the trivial wave is stable in the full three-species system, so that small perturbations in w decay back to zero. If the perturbation in w is above a certain threshold, then the resulting profile will be more similar to a perturbed stable non-trivial wave. As a consequence, the interface will tend to that wave's shape and w will be able to survive near the interface. The unstable non-trivial wave acts like a *separator* between these two different behaviours. We remark that while single interfaces can only behave like either a trivial wave or a stable non-trivial wave, when two or more interfaces interact they may behave differently and travel at other velocities, as we will see in later sections.

We have seen that for a certain range of values of r_3 there exist *two stable* front solutions having the same asymptotic boundary conditions but travelling in *opposite* directions. The same also occurs in FitzHugh-Nagumo-like systems where the equivalent of a trivial wave (usually a standing wave) destabilizes by a pitchfork (NIB) bifurcation generating two symmetric branches of non-trivial stable travelling fronts moving in opposite directions [33]. We remark that such a bifurcation is also a drift bifurcation. However, in that case the two stable waves are both

non-trivial, while in our case the trivial wave is stable and only one of the non-trivial waves is stable. A situation much more similar to ours has been recently discovered in a model of dryland vegetation [68]. This model displays a one-species trivial wave describing the expansion of a herbaceous species and a two-species non-trivial wave characterized by the presence of a second species around the front. While in this case the trivial wave is not independent of the free parameter and the two waves propagate in the same direction, the bifurcation diagram is remarkably similar to our case.

Finally, we stress that when $d_1 = d_2 = d_3 = 1$, as is the case in (4), both the trivial and the stable non-trivial one-dimensional travelling waves are *planarly stable* in two spatial dimensions, i.e., their planar extensions are still stable. Nevertheless the system displays very complex spatio-temporal patterns, as shown in Figure 2. This is in opposition with otherwise similar systems, where front instability is needed in order to observe complex behaviours (e.g., in the case of fronts generated by NIB bifurcation, spiral nucleation occurs in presence of front instability [37]). While it is possible for the non-trivial wave to become planarly unstable if the diffusion rates are different enough, in this paper we will not be concerned with such a case.

3 Interaction of stable travelling waves in one dimension

As the starting point for studying the complex spatio-temporal pattern shown in Figure 2, we consider the interaction of the two stable travelling wave solutions with velocities c_{uv} and c_{uvw} in one spatial dimension. Several outcomes are possible, depending on the value of the free parameter r_3.

Remark 2. Strictly speaking, it is not possible to consider the interaction between the trivial and non-trivial waves introduced in Section 2, since they both share the same asymptotic boundary conditions and such conditions differ for $z \to \pm\infty$: if we place them one next to the other the values at the contact point do not match. However, the travelling wave problem given by (2) and (3) is invariant for the transformation $z \mapsto -z$, $c \mapsto -c$. Given a travelling wave solution, by reflecting its profile around the origin and changing its direction of propagation (but not the speed) we have a travelling wave solution which still satisfies (2) with the swapped asymptotic boundary conditions

$$\begin{aligned} \lim_{z\to-\infty}(U,V,W)(z) &= (0,r_2,0), \\ \lim_{z\to+\infty}(U,V,W)(z) &= (r_1,0,0). \end{aligned} \tag{7}$$

Then, the interaction of such a wave with another satisfying the boundary conditions (3) can be considered, since now the ends of the two waves match.

First, we observe that if two waves of the same kind travel in opposite directions and collide with each other, they are always annihilated. The resulting uniform state is $(r_1, 0, 0)$ in the case of trivial waves [57] or $(0, r_2, 0)$ in the case of non-trivial waves.

The interaction between trivial and non-trivial travelling waves yields more interesting results. If r_3 is sufficiently large, the non-trivial wave is the faster of the two. This case and its consequences for the existence of two-dimensional travelling wave solutions have been discussed in [10]. In this paper we are concerned only with values of r_3 for which the trivial wave is faster than the non-trivial wave. Let us consider the situation in which both waves move towards the right, with the the trivial wave approaching the non-trivial one from the left so

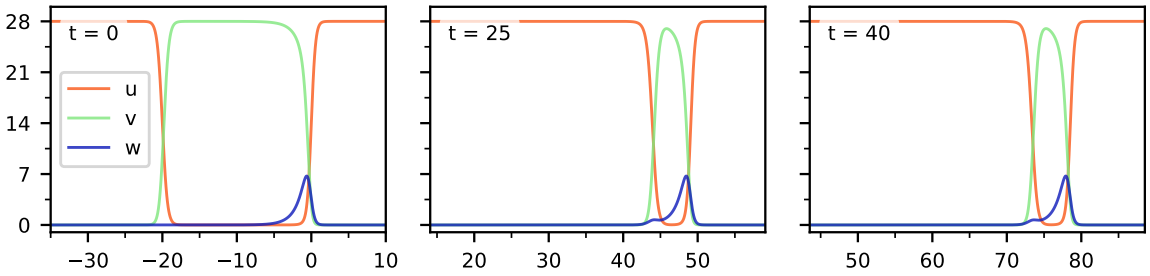


Figure 6 Interaction of the trivial and non-trivial travelling waves for $r_3 = 27.2$, resulting in the waves merging into a single homoclinic travelling wave.

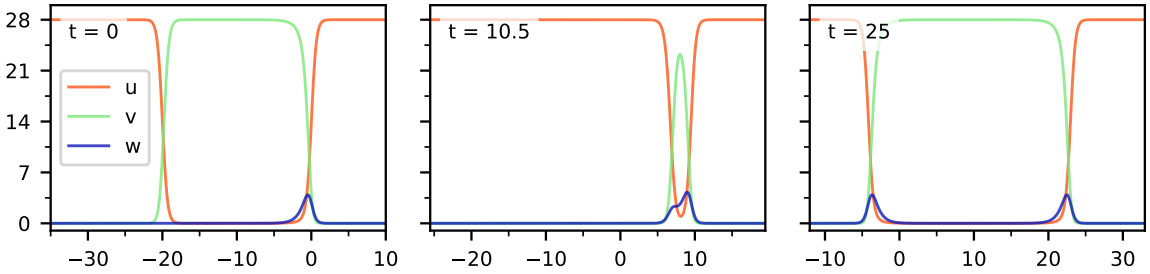


Figure 7 Interaction of the trivial and non-trivial travelling waves for $r_3 = 26.75$, resulting in their reflection, with the trivial wave becoming a non-trivial wave moving in the opposite direction.

that they will collide eventually. The outcome of their collision depends on the relative speed $\Delta c = |c_{uv}| - |c_{uvw}|$ of the fronts, which is itself a function of r_3. In this and later sections, whenever we consider two interacting interfaces between regions where u is dominant and regions where v is dominant, we call *leading front* the interface most advanced in the direction of motion and *back front* the other. In this case, initially the back front is the faster trivial wave, while the leading front is the slower stable non-trivial wave.

If the leftmost trivial wave moves only slightly faster than the non-trivial wave, then after collision the two waves merge and form a single travelling pulse, i.e., a homoclinic travelling wave with the same boundary value at both infinities. An example of such an interaction is shown in Figure 6 for $r_3 = 27.2$, which yields $c_{uvw} \approx -1.96$ and $\Delta c \approx 0.78$ (the corresponding animation can be found at [13]). As the two fronts approach, some of the invading species w moves from the leading front to the back front. Such an influx of w is too small to pass the threshold beyond which the back front would become a non-trivial front, but even a small presence of w reduces the back front velocity, which becomes smaller than the original c_{uv}. On the other hand, as a consequence of the decrease in v due to the interfaces getting closer to each other, w grows in density also around the leading front, increasing its velocity from the original c_{uvw}, albeit only slightly. Once the two fronts are sufficiently near each other, these effects cancel their original speed difference and they propagate like a single travelling pulse at a velocity c_h which is slightly larger than c_{uvw}.

If the relative speed is quite large instead, then after collision the rightmost non-trivial wave continues to propagate unaffected, while the leftmost trivial wave changes nature, becoming a second non-trivial wave moving in the opposite direction as if it were reflected. In this case the

additional influx of w from the leading front to the back front is large enough for the back front to fully become a stable non-trivial front. An example is presented in Figure 7 for $r_3 = 26.75$, which yields $c_{uvw} \approx -0.9$ and $\Delta c \approx 1.85$ (the corresponding animation can be found at [13]). We remark that most of the well-known cases of wave reflection concern the interaction of travelling pulses (see, e.g., [55]), which can reverse their direction of motion by simple reflection of their profile thanks to the fact that the boundary conditions at infinities are the same. Since in our case the interaction occurs between travelling waves with non-matching asymptotic boundary conditions, the reversal of their direction of propagation can be achieved only by a complete change of wave shape and velocity. A similar reflection of fronts was observed in [33, Figure 15(b)] in the context of NIB bifurcations and showed two Bloch fronts of the same kind moving towards each other and transforming into two rebounding Bloch fronts of the other type after collision.

4 Homoclinic travelling waves in one dimension

In the previous section, we observed that the two different types of stable travelling waves of (CD) may merge into a single homoclinic travelling wave with velocity c_h if their speed difference is small. The profile $(U, V, W)(z)$ of this homoclinic wave solves the travelling wave equation (5) with $c = c_h$ and satisfies the asymptotic boundary conditions

$$\lim_{z \to \pm\infty} (U, V, W)(z) = (r_1, 0, 0).$$

Unfortunately, there is no analytical proof of the existence of this solution at the moment. Therefore, we rely on AUTO to continue this solution numerically as r_3 varies, starting from the profile obtained in the simulation of Figure 6. The resulting global structure of the homoclinic travelling wave solution is drawn in Figure 8. As it was the case for the non-trivial wave, its velocity c_h depends on the free parameter r_3. Spatial profiles of the homoclinic wave for some values of r_3 are plotted in Figure 9.

On its right side, the solution branch appears to start from a homoclinic gluing bifurcation at $r_3 = r_G \approx 27.845$, the value of r_3 for which the trivial and non-trivial travelling waves have the same speed, i.e., $c_{uv} = -c_{uvw}$ and $\Delta c = 0$. This bifurcation concerns the travelling waves seen as heteroclinic/homoclinic orbits of a finite dimensional vector field and not as solutions of a time-evolution problem for a reaction-diffusion system. Moreover, strictly speaking, the waves under considerations are not the trivial and the non-trivial waves: the trivial wave must be substituted by the wave obtained by reflection around the origin, as described in Remark 2. The velocity of such a wave is $-c_{uv}$ (which at the bifurcation point has the same sign *and* modulus as c_{uvw}) and its asymptotic boundary conditions are as in (7).

Then, at $r_3 = r_G$ we have two different heteroclinic orbits for the same set of parameters (*including* the wave velocity), both of them connecting the equilibria $(r_1, 0, 0)$ and $(0, r_2, 0)$ but oriented in different directions. While there is no homoclinic orbit connecting $(r_1, 0, 0)$ with itself at $r_3 = r_G$, under some hypotheses a branch of such solutions will be born on one side of the bifurcation point (for mathematical details concerning this and other related bifurcations, such as the homoclinic doubling bifurcation, we refer to [48]). This homoclinic orbit corresponds to the travelling pulse shown in Figure 9. Moreover, since near the bifurcation point the homoclinic orbit must closely follow the two heteroclinic orbits, for values of r_3 very close to r_G the homoclinic wave profile looks like a trivial wave glued together with a non-trivial wave, as shown in Figure 9 (bottom-right panel). Such a gluing of waves is already well known

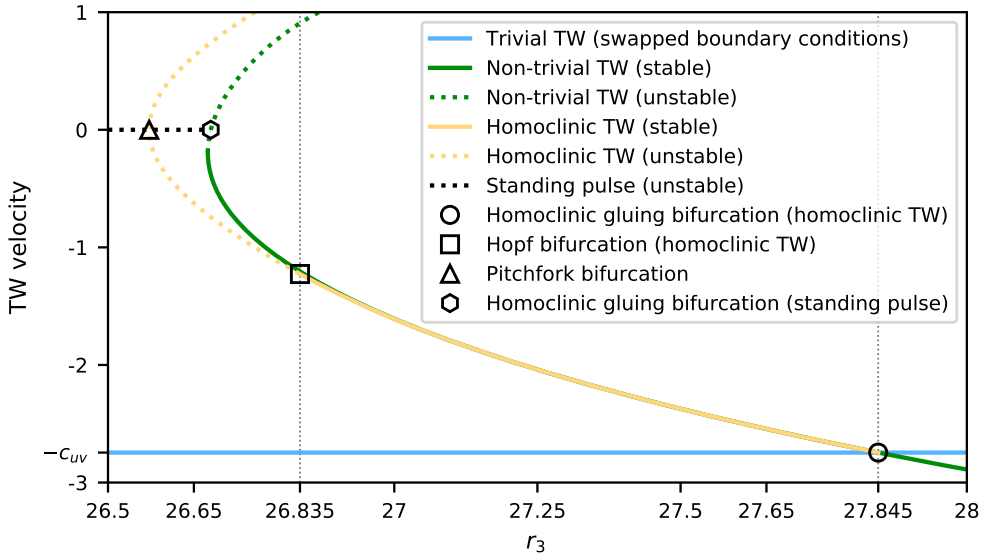


Figure 8 Bifurcation diagram for the one-dimensional travelling fronts and pulses of (CD). The travelling wave velocity is plotted as a function of the free parameter r_3.

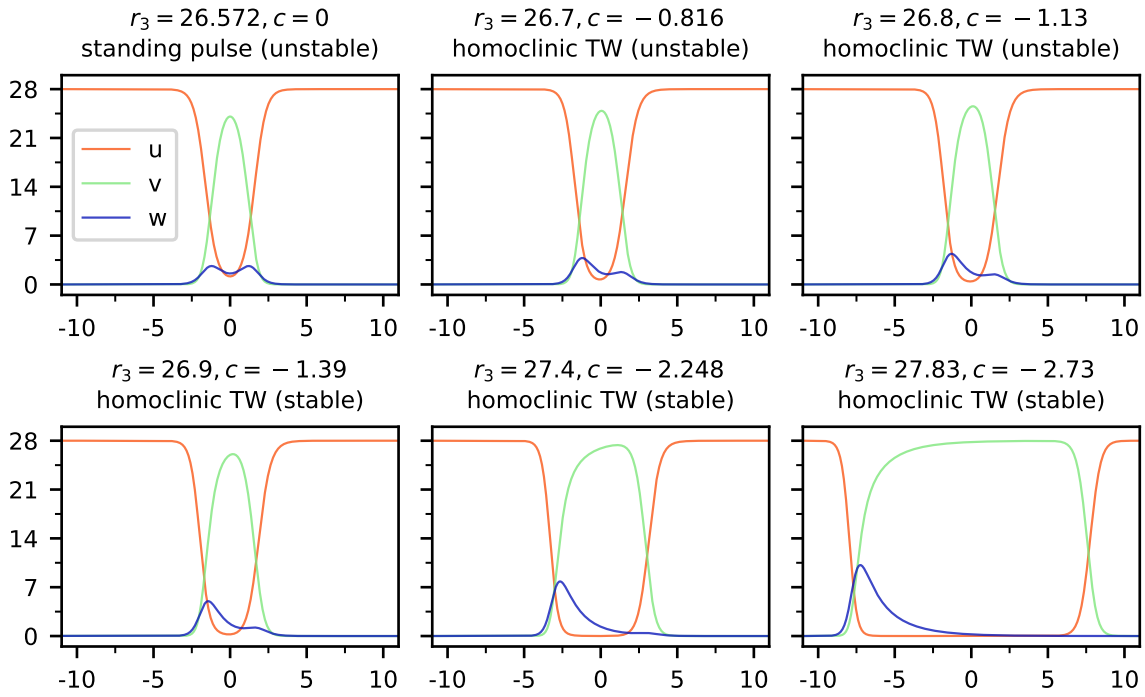


Figure 9 Profiles of the one-dimensional homoclinic travelling wave solutions of (CD), for different values of the free parameter r_3 and corresponding wave velocities c. Negative propagation velocities mean that the pulse is moving leftward.

in the literature. In particular, in [49, 34, 42] the gluing of the two non-trivial fronts originating from NIB bifurcation in FitzHugh-Nagumo-like systems is studied, in [65] the gluing of two unstable fronts is shown to produce a stable pulse, and in [29] the more complicated gluing of a travelling front with a pattern-forming front is considered. Finally, we remark that, in accordance to the properties of homoclinic gluing bifurcations, we expect a second homoclinic orbit to be generated at $r_3 = r_G$. This second orbit should connect $(0, r_2, 0)$ with itself, but we believe the associated travelling pulse to be unstable, since we were not able to observe it numerically. Further study is needed in order to uncover its nature and global structure.

As we have observed in the previous section about travelling wave interaction and can also be seen clearly from Figure 9 (bottom-right panel), the pulse is composed of two distinct interfaces between regions where either $u > v$ or $u < v$, the leading and the back fronts (in Figure 9 the leading front is the leftmost one since the velocity of propagation c_h is negative). Near the homoclinic gluing bifurcation, the leading front resembles the slower non-trivial wave, while the back front resembles the faster trivial wave (with swapped boundary conditions; see Remark 2). However, due to immigration from the leading front, a small amount of the invading species w is present also around the back front, reducing its velocity and preventing it to collide with the leading front. As r_3 decreases the speed difference between the trivial and the non-trivial waves increases, so that the back front must get closer to the leading front to allow the influx of w to be strong enough to equilibrate the velocities of the two fronts. This means that, as we get further away from the homoclinic gluing bifurcation, the width of the pulse becomes smaller and the peak of w around the back front becomes larger, as can be seen from the wave profiles in Figure 9. Moreover, as the pulse width becomes smaller, the density of the species v around the leading front decreases. Since v is stronger than w in the competition as per hypothesis (A3), its decay allows the invader w near the leading front to grow more than it would be possible in a normal non-trivial front. Since to higher densities of w near the interface it corresponds a faster propagation speed, the velocity of the leading front, and thus of the homoclinic travelling wave, is always greater in modulus than the velocity of the stable non-trivial wave, i.e., $c_h < c_{uvw}$. Since the pulse width shrinks as r_3 decreases, the difference between the velocities of the homoclinic and stable non-trivial waves increases as r_3 decreases, as can be seen in the bifurcation diagram of Figure 8.

As for the stability of the homoclinic travelling wave, for values of r_3 sufficiently near to r_G it can be verified numerically that the wave is stable. These are the values of r_3 for which the collision of trivial and non-trivial waves results in their merging into a single pulse, as previously shown in Figure 6. However, at a certain point $r_3 = r_H \approx 26.83586$ the homoclinic wave goes through a Hopf bifurcation and loses stability. The behaviour of travelling wave interaction after the Hopf bifurcation will be studied later in Section 6.

Once r_3 reaches the value $r_3 = r_P \approx 26.572$, the velocity of the travelling pulse becomes zero and the corresponding wave profile is symmetric, as shown in Figure 9 (top-left panel). This point is a pitchfork bifurcation, where the asymmetric travelling pulse branches off a symmetric standing pulse solution (i.e., a travelling pulse with zero velocity). Since for a pulse the boundary conditions at infinities are the same, on the other side of the standing wave branch there is a second asymmetric travelling pulse branch, which is exactly the reflection of the first one around the axis $c = 0$.

As for the standing pulse solution, we believe that it is generated at $r_3 = r_{G'} \approx 26.679$ from a degenerate homoclinic gluing bifurcation associated to two zero-velocity unstable non-trivial travelling waves oriented in opposite directions. Its initial profile can be seen in Figure 10 (rightmost panel). Note that the point at which the non-trivial wave has zero velocity *is not*

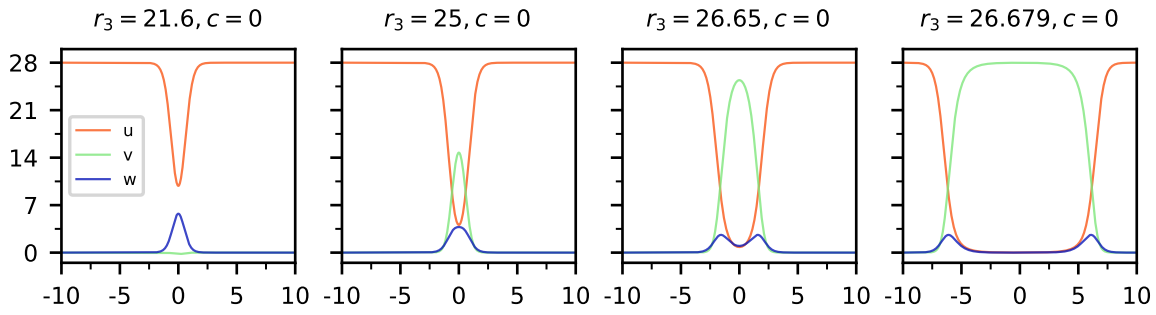


Figure 10 Profiles of the one-dimensional standing pulse solutions of (CD), for different values of the free parameter r_3. Note that in the leftmost panel the species v assumes negative density values and the pulse is thus inadmissible from a modelling point of view.

the fold bifurcation of its branch. As r_3 decreases, the pulse shrinks, as shown in Figure 10 (third and second panels), until its profile is no longer non-negative and the wave becomes non-admissible from a modelling point of view, as shown in Figure 10 (leftmost panel). All along its branch, this standing wave solution is unstable. Probably for this reason, it does not appear to play an important role in the patterns displayed by this system and we will not be concerned with it any further in this paper.

5 Breathing travelling waves

In the previous section we showed how the homoclinic travelling wave solution is destabilized through a Hopf bifurcation, as shown in the bifurcation diagram of Figure 8. When a dynamical system goes through a Hopf bifurcation a periodic orbit is generated and this section will be devoted to studying such a periodic solution and its bifurcation structure.

Let us consider the time-evolution problem associated to the travelling wave equation (5):

$$\begin{cases} U_\tau = d_1\, U_{zz} + c\, U_z + (r_1 - U - b_{12}\, V - b_{13}\, W)\, U, \\ V_\tau = d_2\, V_{zz} + c\, V_z + (r_2 - V - b_{21}\, U - b_{23}\, W)\, V, \\ W_\tau = d_3\, W_{zz} + c\, W_z + (r_3 - W - b_{31}\, U - b_{32}\, V\,)\, W, \end{cases} \tag{8}$$

where the profile $(U, V, W)(z, \tau)$ now also depends on a time variable τ. We remark that (8) is equivalent to considering the competition-diffusion system (CD) on the real line and in a reference frame moving with velocity c. Then, the profile of the homoclinic travelling wave of (CD) is a stationary solution of (8) when $c = c_h$, with c_h being the velocity of the homoclinic wave. As we have seen in the previous section, at $r_3 = r_H$ this solution goes through a Hopf bifurcation and loses stability. Then, we can expect that a time-periodic solution of (8) is generated on one side with respect to r_H. We will denote by T the period of such a solution and by c_b the velocity of the reference frame; both quantities depend on the free parameter r_3. The initial values of c_b and T at $r_3 = r_H$ are expected to be equal to c_h and $2\pi/\omega \approx 5.377$ respectively, where $\omega \approx 1.169$ is the modulus of the imaginary part of the couple of eigenvalues crossing the imaginary axis at the Hopf bifurcation.

In the fixed frame of reference, this solution appears like a travelling wave whose profile oscillates periodically. It can be written as $(u, v, w)(x, t) = (U, V, W)(x - c_b\, t, t)$, where c_b is

the wave velocity and $(U, V, W)(z, \tau)$ is the travelling wave profile which satisfies (8) with $c = c_b$ and is T-periodic in the time variable τ. In particular, in this case it is the pulse width that oscillates periodically, which earned the name of *breathing travelling waves* (or *travelling breathers*) for solutions of this type (see, e.g., [43]). If the wave velocity c_b is zero, then we have standing breathers such as those observed in the case of a FitzHugh-Nagumo-like system with NIB bifurcation [33, Figures 14 and 15(a)]. We remark that c_b is the mean velocity of the wave over time-intervals of length T. The instantaneous front velocity may differ from c_b and is in general a T-periodic function of time.

In Figure 11 we plot the period T and mean velocity c_b of the breathing wave as functions of r_3, as obtained by numerical continuation. The period T seems to go to infinity at one end of the branch, making the numerical solution increasingly difficult to obtain. Moreover, we observe that it holds $|c_h| > |c_b| > |c_{uvw}|$, with c_b starting equal to c_h near the Hopf bifurcation point and apparently tending to c_{uvw} as the period T goes to infinity. As some concrete examples of the breathing travelling wave, we have chosen three values of r_3 and reported the features of the corresponding breathing solutions in Figures 12, 13 and 14. Animations containing the same features for a larger number of values of r_3 can be found online at [12]. First, we focus on the general properties of the breathing wave, shared by all values of r_3. Later we will describe how the breathing wave gradually changes as the free parameter r_3 is decreased.

In Figure 12 we have plotted the breathing wave profile $(U, V, W)(z, \tau)$ over one time period T. Since u and v are essentially complementary, we have used the relative strength indicator $u/(u + v)$ instead of showing both u and v separately. Moreover, since the spatial frame of reference used is moving at the velocity c_b, globally the wave appears to be still. From Figure 12 we can see that also the breathing wave is composed by a back and a leading front (here the leftmost and rightmost fronts respectively), similarly to the homoclinic wave from which it originates. The mean velocity of these two fronts over time intervals of length T is equal to c_b, but their instantaneous velocities are not constant and are plotted in Figure 13. As a means of comparison, the *unsigned* speeds of the other travelling waves are also plotted. For the fronts of the breathing wave the signed velocity is instead used, showing that they are always moving in the same direction. In Figure 12 the back front appears to move backwards to the left for some time, but this motion is relative to the reference frame moving with the mean breathing wave velocity c_b. In the fixed reference frame both the leading and the back fronts are always moving forward to the right.

The breathing wave cycle can be divided into two phases. In the first one, the back front is slower than the leading front, thus causing the distance between the fronts, i.e., the pulse width, to increase. The second phase sees the back front becoming faster than the leading front and the pulse width shrinking as a consequence. This is possible since the amount of the species w around the back front appears to be greatly reduced compared to the first phase (especially as we get further away from the Hopf bifurcation), thus increasing the back front velocity. Also note that both the maximum pulse width and the period T increase as we move along the solution branch.

Compared to the back front, the instantaneous velocity of the leading front oscillates around c_b weakly. In order to appreciate its oscillation, we have provided enlargements in the second row of Figure 13. The maximum velocity is achieved some time after the minimum pulse width has been attained, because, due to the small pulse width, the density of the species v around the leading front is reduced. Since v is stronger than w as per hypothesis (A3), its reduction favours the invading species w and brings about a small increase in its density around the leading front, which then becomes slightly faster.

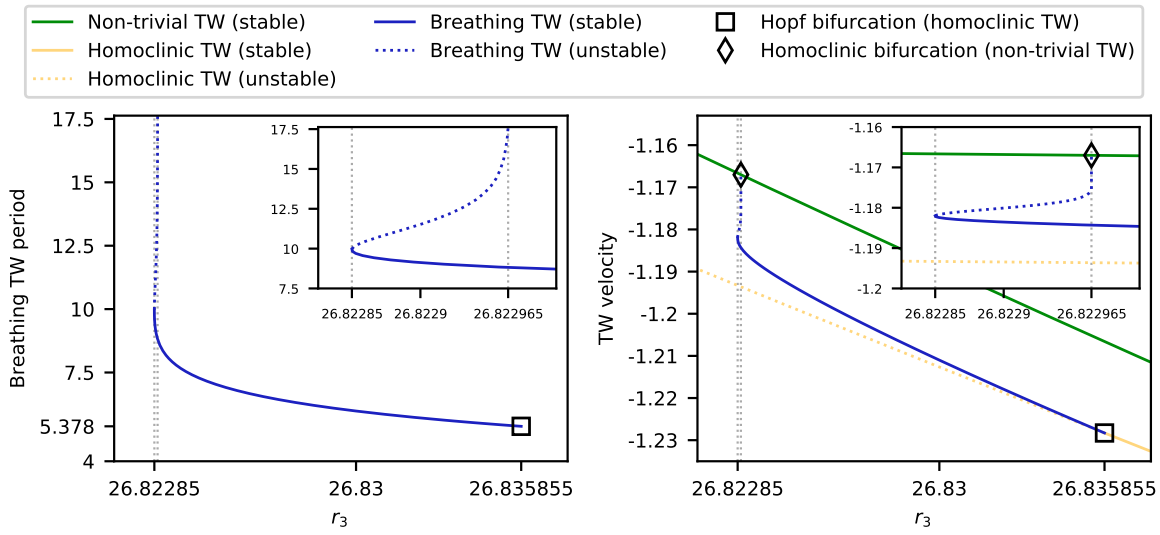


Figure 11 Global structure of the breathing travelling wave solution. Its period T (left panel) and its mean velocity c_b (right panel) have been plotted as functions of the free parameter r_3. Details of the unstable branch are also present.

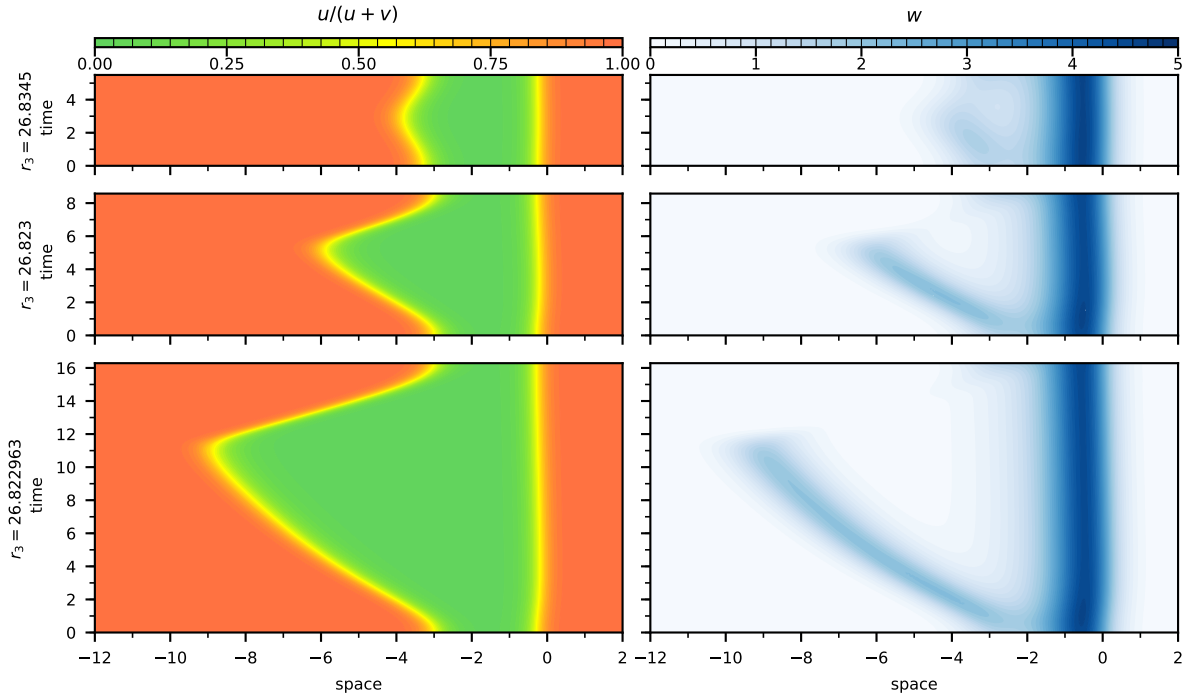


Figure 12 Space-time profiles of the breathing travelling wave over one time period T for three different values of r_3. Instead of plotting u and v separately, we have used $u/(u+v)$ as a measure of the relative strength of u and v. The spatial frame of reference moves at the velocity c_b, the mean velocity of the breathing wave.

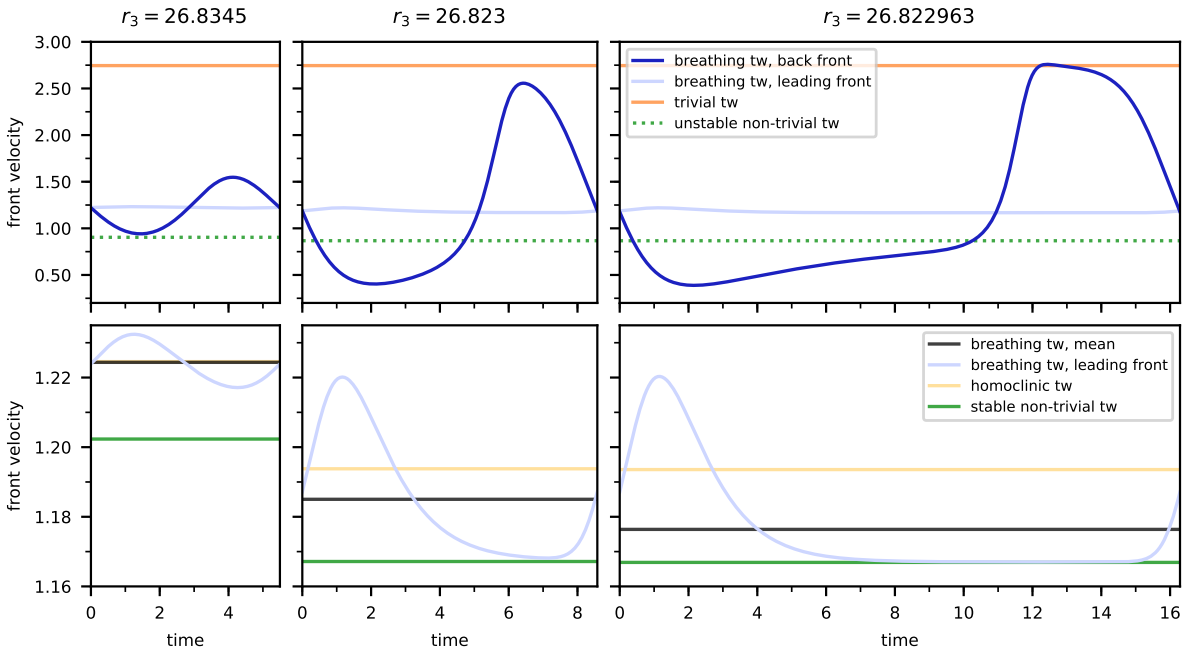


Figure 13 Temporal profiles of the instantaneous velocities of the back and leading fronts of the breathing travelling wave for three different values of r_3. The unsigned speeds of the other types of travelling waves are also plotted for comparison.

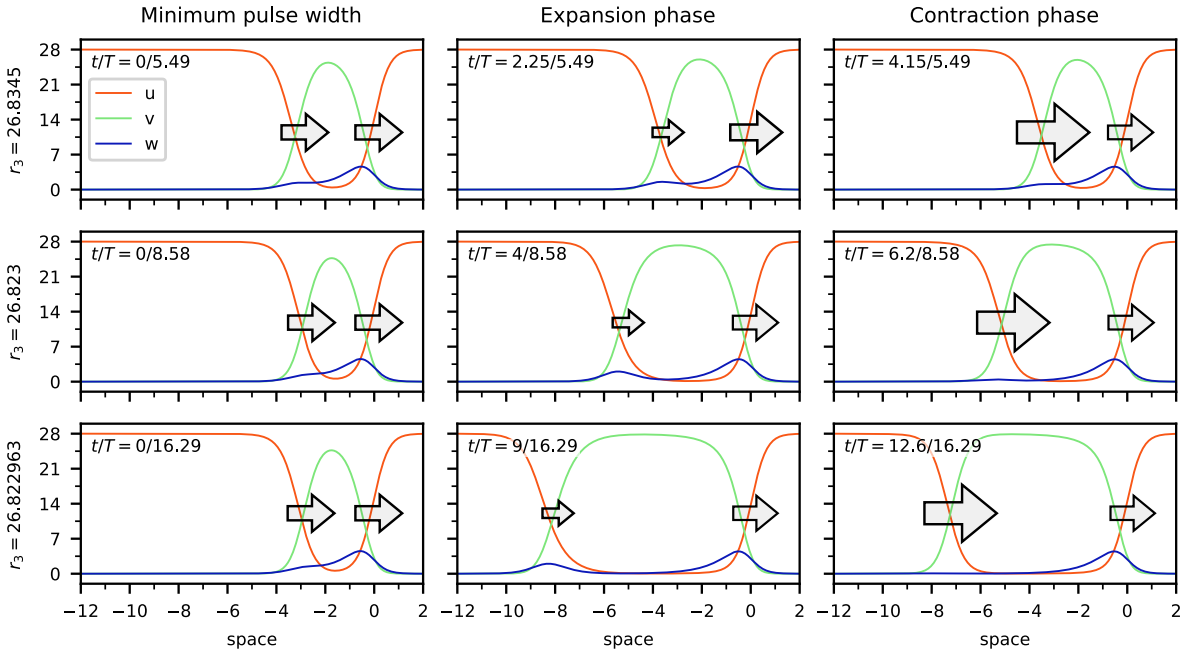


Figure 14 Spatial profiles of the breathing travelling wave during the expansion and contraction phases for three different values of r_3. The spatial frame of reference moves at the velocity c_b, the mean velocity of the breathing wave. The arrows show the direction of propagation and the speed of the two fronts.

Finally, in Figure 14 we show the spatial profile of the breathing wave at three different time instants. The first column shows the time at which the pulse width is the shortest. Note how at this time the velocities of the leading and back fronts are the same and how the wave profile is quite similar to that of the homoclinic wave. In the second column, a snapshot of the expansion phase of the pulse width is shown, where the velocity of back front becomes smaller than the velocity of the leading front. In the last column, the contraction phase is depicted, in which the back front becomes faster than the leading front.

Now, we follow the evolution of the breathing travelling wave along its solution branch, as plotted in Figure 11. We start from the vicinity of the Hopf bifurcation point, for example taking $r_3 = 26.8345$, for which $T \approx 5.49$ and $c_b \approx 1.224$, as shown in the first row of Figures 12 and 14 and in the first column of Figure 13. In this case the breathing wave does not deviate too much from the homoclinic wave, either in profile or velocity. The back front velocity does not oscillate very far from the mean velocity c_b and the reduction of the density of w around the back front during the contraction phase is not very significant. In particular, at all times the area where w is non-negligible straddles both fronts, connecting them as in the homoclinic wave.

As r_3 decreases, the maximum pulse width increases and so does the time-period T. As an example, we consider $r_3 = 26.823$, for which $T \approx 8.58$ and $c_b \approx 1.185$, as shown in the second row of Figures 12 and 14 and in the second column of Figure 13. Now we will describe in detail the behaviour of this solution for one time period.

At the instant of shortest pulse width, the breathing wave profile is still very similar to the homoclinic wave and the same can be said for the velocity of both back and leading fronts. Then, the pulse width increases and compared to the previous case ($r_3 = 26.8345$) the two interfaces travel further away from each other and the two peaks of w around them become more clearly separated.

In the expansion phase, the leading front looks quite similar to the stable non-trivial travelling wave with velocity c_{uvw}. Just after the minimum pulse width is reached, its speed is slightly larger than $|c_{uvw}|$, and even larger than the homoclinic wave speed $|c_h|$, due to the reduced density of v caused by the small pulse width. As the distance between the fronts increases this effect becomes weaker, so that velocity and profile of the leading front approach those of the stable non-trivial wave. On the other hand, in the expansion phase the back front resembles the unstable non-trivial travelling wave. Similarly to the leading front, at the beginning of the expansion phase the peak value of w near the back interface is slightly higher than that of the unstable non-trivial wave, but as time progresses it decays slowly and the velocity of the back front tends to that of the unstable non-trivial wave.

Due to the unstable nature of such a wave, at a certain point the species w around the back front dies out quite abruptly. As a consequence, the back front accelerates, becoming faster than the leading front and marking the beginning of the contraction phase of the pulse width. In this phase, the back front becomes similar in appearance and velocity to the trivial travelling wave, while the leading front is still resembling the stable non-trivial wave. When the two fronts are sufficiently near for w to colonize again the back front, the back front slows down and matches in speed the leading one, bringing us back to the starting point. Thus, the behaviour of the breathing wave may also be described as some kind of imperfect or incomplete reflection: a faster trivial wave collides with a slower stable non-trivial wave, then is "reflected" without changing direction of motion as an even slower unstable non-trivial wave, eventually decays back to a trivial wave and the cycle starts again from the beginning.

As r_3 continues to decrease, the back front travels further backward before destabilizing,

leading to an increase in period and maximum pulse width. At $r_3 = r_{BF} \approx 26.82285$, the breathing travelling wave undergoes a fold bifurcation and disappears. However, using numerical continuation we can follow the unstable branch, for which the period T increases as r_3 increases, as can be seen in the detail panels of Figure 11. Solutions on the unstable branch have the same qualitative behaviour as those on the stable branch, but the maximum front separation and increase in period become even more dramatic. As an example, we consider the unstable breathing wave for $r_3 = 26.822963$, with $T \approx 16.29$ and $c_b \approx 1.176$, as shown in the third row of Figures 12 and 14 and in the third column of Figure 13. Note how the decay in the density of w around the back front during the expansion phase is much slower, allowing the fronts to travel further away from each other until they look like two separate waves. The fraction of the period in which the back front resembles either the unstable non-trivial wave or the trivial wave becomes larger. Similarly, the leading front behaves like the stable non-trivial wave for a longer time and consequently the mean breathing wave velocity will get away from the homoclinic wave velocity and approach the velocity of the stable non-trivial wave, as can be seen in the right panel of Figure 11.

While numerical computation becomes increasingly difficult as the time-period T increases, it appears that T tends to infinity as r_3 tends to a certain value $r_{HC} \approx 26.822965$. Since the maximum pulse width increases together with the period, we expect the maximum distance between the fronts to also tend to infinity, while the breathing wave velocity c_b should tend to c_{uvw} since the leading front behaves like a stable non-trivial wave for most of the time. Since the period goes to infinity, the time-periodic breathing travelling wave solution tends to an entire solution of (8), i.e., a solution defined for all times $\tau \in \mathbb{R}$. Moreover, since the two fronts get arbitrarily far away from each other, it appears that this entire solution describes the interaction of a faster trivial wave with a slower stable non-trivial wave. After interaction, the back front slows down without changing direction, its shape and velocity tending to those of an unstable non-trivial wave as the time goes to infinity. On the other hand, the leading stable non-trivial wave is essentially unaffected by the collision. In particular, since the moving frame is centred on the leading front, in the entire solution the spatial profile will tend pointwise to the profile of the stable non-trivial wave as the time goes to $\pm\infty$. In other words, for $r_3 = r_{HC}$ it seems that we have a homoclinic bifurcation in the system (8), for the equilibrium given by the stable non-trivial travelling wave, the homoclinic orbit at $r_3 = r_{HC}$ given by the entire solution described above and the periodic orbit for $r_3 < r_{HC}$ given by the breathing travelling wave.

As we will see in the next section, in numerical simulations the interaction of a trivial wave with a stable non-trivial wave either results in two stable non-trivial waves for $r_3 < r_{HC}$ or in a single pulse for $r_3 > r_{HC}$. This suggests that the entire solution associated to the homoclinic bifurcation must be unstable, since we never observe the back front becoming an unstable non-trivial wave. Confirming the existence of such a solution at $r_3 = r_{HC}$ and studying its evolution as r_3 is varied are still open problems, both analytically and numerically. We believe that reducing the wave interaction problem to a system of ordinary differential equations by a singular limit procedure may allow the problem to become more tractable.

Finally, for a description of a similar bifurcation structure for a different type of time-periodic solutions occurring in another reaction-diffusion system, along with details about the numerical methods needed for the numerical continuation of such solutions, we refer the interested reader to [59].

6 The mechanism behind travelling wave reflection

Going back to the problem of one-dimensional travelling wave interaction presented in Section 3, we discover that the homoclinic and breathing travelling wave solutions we have studied in Sections 4 and 5 respectively are deeply linked with the transition from the merging-after-collision regime of Figure 6 to the reflection regime of Figure 7. This is not completely unexpected, since for example it is known that unstable twin-peaked solutions called scattors have a fundamental role in the interaction of travelling pulses in the Gray-Scott model [60].

First, we slightly perturb the homoclinic travelling wave and see how the resulting wave evolves with time. Clearly, if r_3 is larger than the Hopf bifurcation point r_H, then the homoclinic wave is stable: the perturbation simply decays to zero and the wave reverts to its original shape. If $r_{BF} < r_3 < r_H$ the homoclinic wave is unstable, but a stable breathing wave does exist. Then, in this parameter range, the distance between the back and leading fronts of the perturbed pulse starts oscillating and the solution tends to the breathing wave. If $r_F < r_3 < r_{BF}$ no breathing wave exists and the back front, after oscillating for a while, reverses its direction of propagation. The end result consists in two stable non-trivial waves moving in opposite directions, as can be seen in Figure 15 for the example value $r_3 = 26.75$ (the corresponding animation can be found at [16]). If $r_3 < r_F$ then the non-trivial fronts no longer exist and the homoclinic wave decays to the homogeneous state $(r_1, 0, 0)$.

Outcomes of pulse destabilization and travelling wave interaction are similar. In fact, when the trivial wave approaches the slower non-trivial wave their combined profile becomes pulse-like in appearance, i.e., a sort of perturbation of the homoclinic wave. As a consequence, the result of the interaction is determined by the fate of the perturbed pulse. We checked this hypothesis by numerical simulation, finding it true outside the region of existence of the unstable breathing wave ($r_{BF} < r_3 < r_{HC}$). Examples of wave reflection for $r_3 < r_{BF}$ and wave merging for $r_3 > r_H$ have already been shown in Figures 7 and 6 respectively. In Figure 16 we show an example in which the colliding waves merge into the stable breathing travelling wave for $r_3 = 26.823 \in (r_{HC}, r_H)$ (the corresponding animation can be found at [13]).

In the region $r_{BF} < r_3 < r_{HC}$ a perturbed homoclinic wave becomes a breathing wave, but the interaction of the trivial and non-trivial waves results in reflection, as can be seen in Figure 17 for $r_3 = 26.8229$ (the corresponding animation can be found at [13]). We believe this discrepancy is due to the existence of the unstable branch of the breathing travelling wave, which acts as a separator between the stable breathing wave and the reflection-like behaviour. An indication of this fact can be seen by looking closely at Figure 17. After the waves collide, the back front does not immediately change direction of propagation, but slows down first, resembling an unstable non-trivial wave. This is the same behaviour we observed in the expansion phase of the unstable breathing wave of Figure 12 (third row). While in the unstable breathing wave the exotic species w present near the back front decays eventually and two fronts approach again, in the case of interacting waves the back peak of the density w grows to the full size observed in a stable non-trivial wave and the back front starts to move backwards. As a comparison, in Figure 18 we have plotted the space-time profile of the reflection of travelling waves in the case $r_3 = 26.75$, when there is no unstable breathing wave. In such a case, after collision the back front changes direction of propagation immediately, skipping the intermediate phase in which the behaviour is similar to that of the unstable breathing wave.

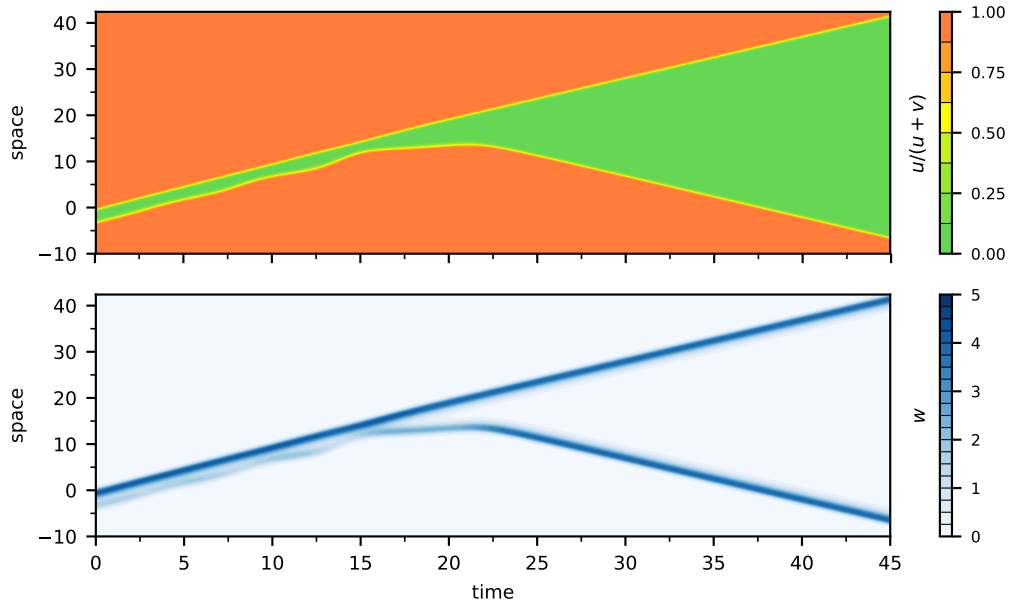


Figure 15 Perturbing an unstable homoclinic wave for $r_3 = 26.75$ results in two stable non-trivial fronts moving in opposite directions.

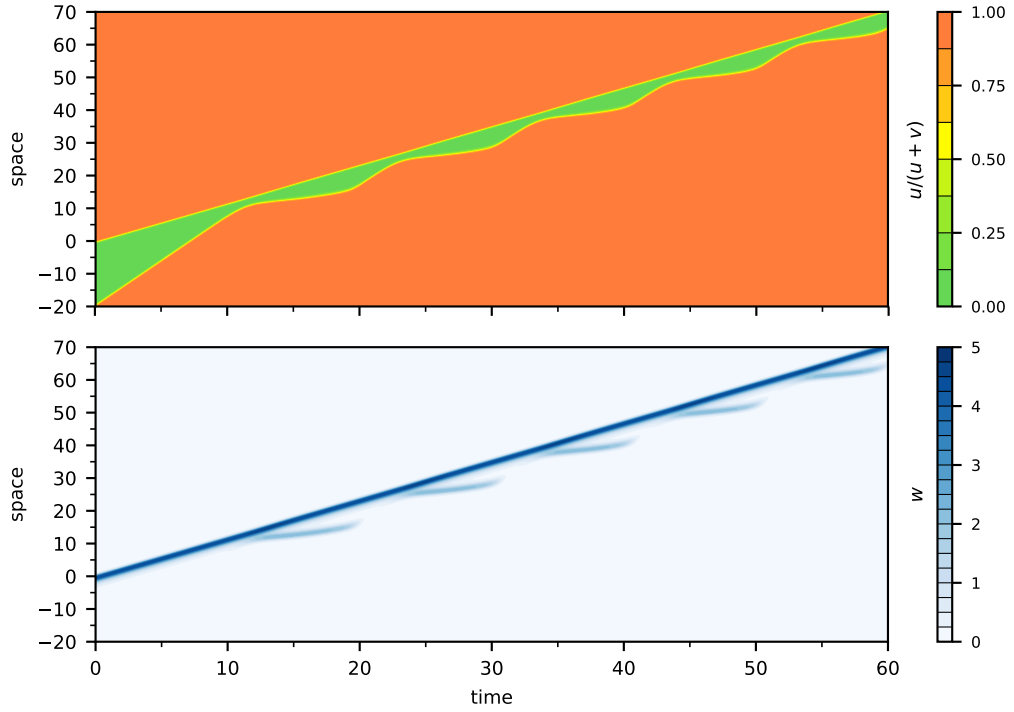


Figure 16 Interaction of the trivial and non-trivial travelling waves for $r_3 = 26.823$, resulting in the waves merging into the stable breathing travelling wave.

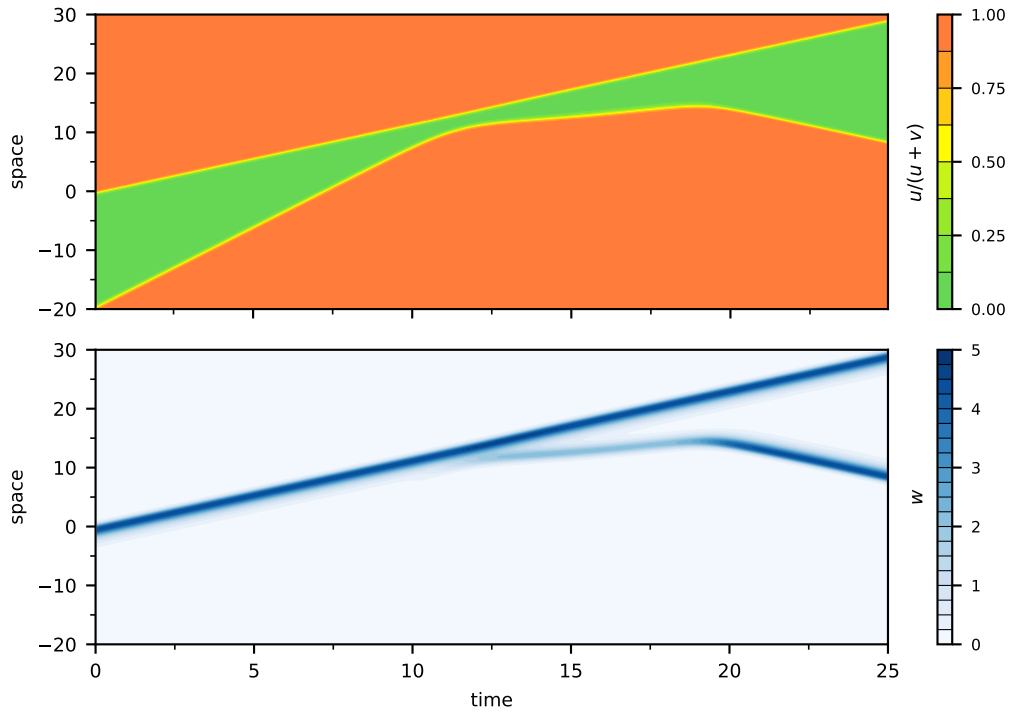


Figure 17 Interaction of the trivial and non-trivial travelling waves for $r_3 = 26.8229$, resulting in their reflection. The unstable breathing wave exists for this value of r_3.

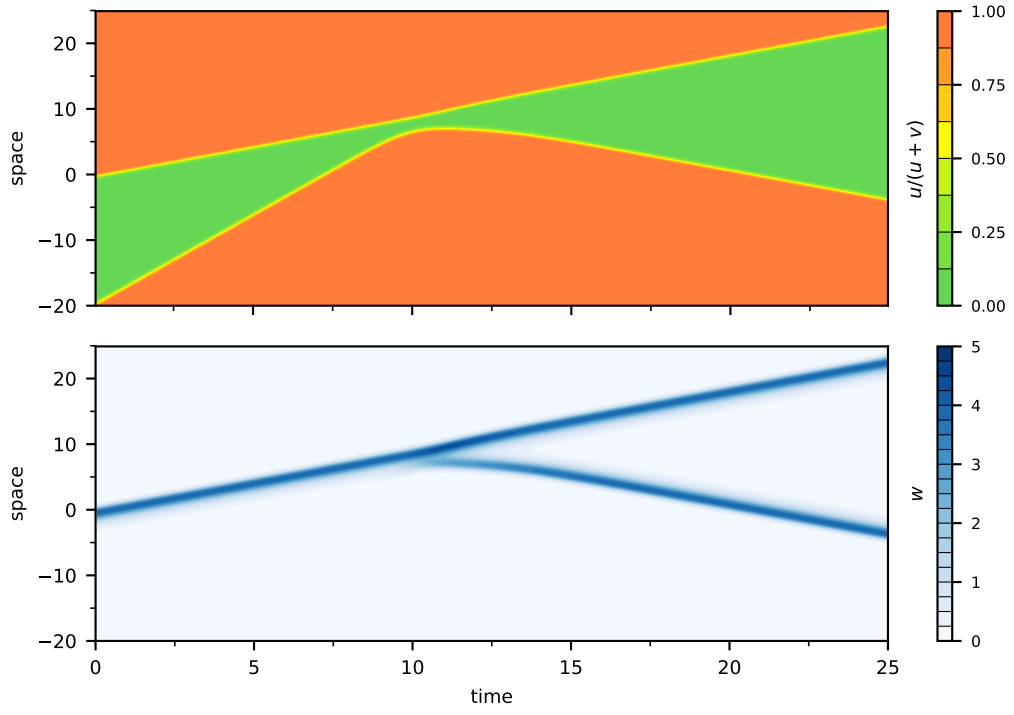


Figure 18 Interaction of the trivial and non-trivial travelling waves for $r_3 = 26.75$ (same simulation of Figure 7), resulting in their reflection. No breathing wave exists for this value of r_3.

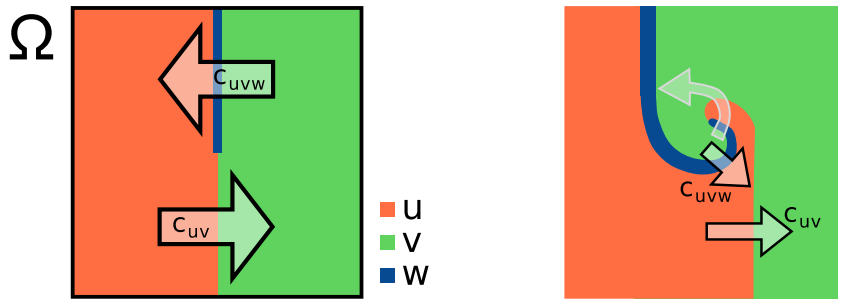


Figure 19 Left panel: Initial conditions for the interaction of non-trivial (top half-region) and trivial (bottom half-region) waves in a square domain Ω. Right panel: Tip formation and movement when $|c_{uvw}| < |c_{uv}|$. Arrows outlined in black denote the front velocities, while the arrow with white outline shows the tip movement, which leads the tip front to collide with the tip back.

7 Interaction of stable trivial and non-trivial planar waves in two dimensions

In order to explain the origin of the complex spatio-temporal pattern shown in Figure 2, in this section we study the interaction of the planar extensions of the trivial and non-trivial stable travelling waves introduced in Section 2. As we have already observed, these two planar waves are stable in two spatial dimensions for the parameter values satisfying (4).

As a simplified initial condition, in a square domain Ω we place the non-trivial wave in the upper half-region and the trivial wave in the lower half-region, as shown in Figure 19 (left panel). The planar front velocities are respectively c_{uvw} and c_{uv}, where $c_{uvw} < 0$ varies with r_3 and $c_{uv} \approx 2.575 > 0$ is independent of r_3 instead. Then, the non-trivial planar wave moves to the left in the upper part, while the trivial wave moves to the right in the lower part. This two-dimensional initial condition for the trivial and non-trivial fronts is equivalent to the one shown in [19, Figures 9 and 10], where the interaction of two Bloch fronts, resulting in the appearance of a spiral pattern, was considered in a system of forced coupled oscillators.

In order to similarly observe in our system the appearance of a rotating tip at the point of contact of the two planar waves, we will restrict ourselves to values of r_3 for which $|c_{uvw}| < |c_{uv}|$. Then, the slower non-trivial wave makes up the back of this tip while the faster trivial wave makes up its front, as shown in Figure 19 (right panel). As a consequence, the front of the tip will eventually collide with its back. From our observations in one spatial dimension presented in Section 3, we expect the results of this collision to depend on the relative velocity of the interacting fronts. While in one spatial dimension the relative velocity of the fronts depends only on r_3, in two (and above) dimensions it depends also on the curvature of the fronts, so that interacting fronts do not always behave similarly even if r_3 is the same. We have already observed this phenomenon in our previous study of two-dimensional travelling waves of the three-species competition-diffusion system [10].

We also remark that, in order to keep computation time reasonable, the spatial discretization used in our simulations is rougher in two dimensions than in one dimension. In particular, we have chosen a regular rectangular grid with step size $\Delta x = 0.1$. Due to the different spatial resolution, the exact values of r_3 at which the transitions between the different regimes occur will be different. However, as far as we can tell, the qualitative behaviour does not change by further reducing Δx. Moreover, if Δx is too large (e.g., $\Delta x = 0.2$), the anisotropy in

the discretization between directions parallel and diagonal to the axes will lead to a strong anisotropy in the front velocities. This anisotropy can generate artefacts that destabilize the fronts. In our future work, by applying a more sophisticated numerical method than finite differences, we intend to simulate the two dimensional behaviour more precisely. In particular, since the densities are essentially constants away from the moving interfaces, adaptive mesh refinement seems to be a compelling option, possibly using a posteriori error estimates such as those recently proposed in [7].

We have plotted the results of the numerical simulations with the initial conditions of Figure 19 (left panel) in Figures 20–24. The corresponding animations can be found at [14]. First, suppose that r_3 lies in the region where there exists a stable homoclinic travelling wave. Then, we can expect the front of the tip to merge with its back when they collide. As can be seen in Figure 20 for the example value $r_3 = 26.9$, this leads to the formation of a steadily rotating spiral similar to those observed in excitable media, such as the well known Belousov-Zhabotinsky chemical reaction [1]. Indeed, if we consider an initial condition equal to $(r_1, 0, 0)$ in the upper half-region and equal to the planar extension of the homoclinic wave in the lower part, the end result is still a stable spiral. Such initial conditions correspond to "cutting" a front with an obstacle in the Belousov-Zhabotinsky reaction, which is one of the standard methods used to obtain a spiral core. Stable regular spiral waves also appear in systems with NIB bifurcations. The case of forced coupled oscillators was studied in [19] for the same initial conditions as ours, while kinematic equations for the front motion in FitzHugh-Nagumo-like systems were obtained in [37, 36] by singular perturbation in the vicinity of the bifurcation and also showed the appearance of spiral patterns.

When r_3 decreases, the homoclinic wave destabilizes by Hopf bifurcation and a stable breathing wave appears. The front of the tip still merges with its back but the combined pulse breathes. The final result is a spiral whose arm's width is oscillating. When the oscillation is sufficiently small, the coils of the spiral never touch and this breathing spiral appears to be stable. An example for $r_3 = 26.83$ is shown in Figure 21. Note that the arm width oscillates more strongly far away from the core. We believe this is due to the fact that the high curvature of the trivial and non-trivial fronts near the core decreases their relative velocity, promoting their merging into a single pulse. Then, the homoclinic pulse that makes up the spiral arm is more stable near the core and the further it travels the more it oscillates.

It looks like that the regular spiral has destabilized by a Hopf bifurcation generating a periodic pattern as a result, behaving exactly as its one-dimensional counterpart, the travelling pulse (more detailed computations are needed to confirm this intuition). Breathing spirals of this kind are not common in the existing literature. For example, they have been observed in the CDIMA chemical reaction, but only under external periodic forcing [5, 28]. On the other hand, breathing spirals have been shown to exist in absence of external forcing in the Aliev–Panfilov model for the excitation dynamics of the cardiac tissue, but only in annulus domains [63].

If r_3 decreases further, the oscillations become larger and eventually the homoclinic front splits into two non-trivial fronts. Then, the coils of the spiral collide and annihilate, leaving gaps in the spiral arm. This leads eventually to the formation of new spiral cores. An example of this process for $r_3 = 26.8175$ is shown in Figure 22. When the spiral is small, the stabilizing effect of curvature prevents it from breaking. However, the spiral arm already starts to breath, as can be seen in Figure 22 (first panel). When the spiral arm travels further enough from the core, the oscillations become so large that the back front of a coil collides with the leading front of the previous coil, resulting in their annihilation and in a gap in the spiral arm, as can

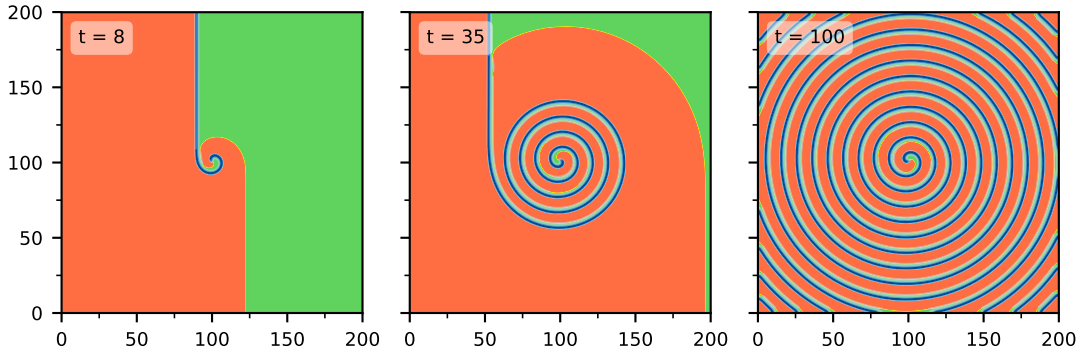


Figure 20 In the case $r_3 = 26.9$, initial conditions as in Figure 19 (left panel) lead to a stable regular spiral.

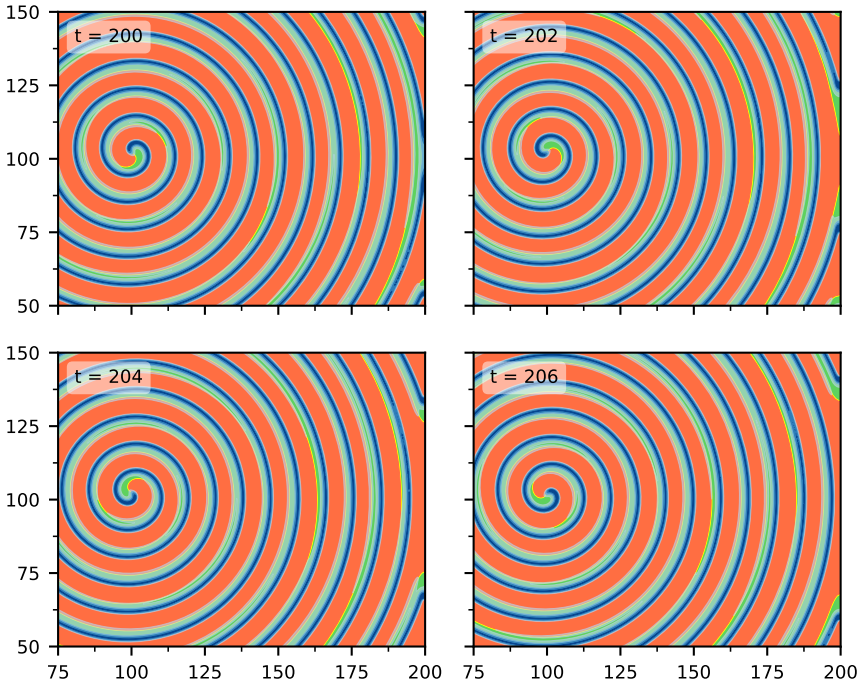


Figure 21 In the case $r_3 = 26.83$, initial conditions as in Figure 19 (left panel) lead to a stable breathing spiral. The initial phase in which the spiral forms is similar to Figure 20. Here we have plotted an enlarged region in order to better see the arm width variations. We encourage the reader to zoom in in the electronic version.

be seen in Figure 22 (panels 2–4). The gap leads to the formation of new spiral cores and the same process repeats itself until a pattern formed by many spirals is obtained, as can be seen in Figure 22 (panels 5–7). The spiral cores are quite stable and do not display meandering. For this reason, after an initial transient phase the number and position of the spiral cores appear to become fixed and the resulting pattern repeats itself periodically in time, as can be seen by comparing the eight and ninth panels of Figure 22.

There are two points we want to highlight. First, the final pattern of the simulation in Figure 22 consists in a large central spiral surrounded by a large number of smaller spirals. Since a spiral can only grow as long as it does not destabilize or collide with another one, only the initial spiral is able to reach its maximum allowed size. The spiral cores generated after its breakdown must compete for space with each other, preventing them from growing as much. Thus, the particular distribution of spiral sizes observed is not general but just a consequence of our choice of the initial conditions. The only quantity independent of the initial conditions (but dependent on r_3) is the maximum size that can be reached by a single spiral. Secondly, spiral breakup occurs only far from the spiral core. It follows that, if the same initial conditions for the same value of r_3 were to be considered in a smaller domain, the resulting pattern would be a breathing spiral such as the one shown in Figure 21. This raises the question of whether breathing spirals can only appear in bounded domains. While rigorously proving the existence of breathing spirals in the whole $\mathbb{R}^2$ is an open problem, we expect them to exist as long as r_3 is chosen sufficiently near r_H, the Hopf bifurcation point of the homoclinic wave.

The mechanism leading to the generation of new spiral cores in Figure 22 appears qualitatively similar to the spiral breakup observed in FitzHugh-Nagumo-like systems [51, 35]. In such cases the breakup of the spiral arm is caused by the planar instability of one of its constituent fronts, as for example it was shown by singular limit analysis for the case of Bloch fronts in [37, 36]. However, in our case both the trivial and non-trivial fronts, as well as the travelling pulse, are planarly stable and thus we expect that breakup is caused by the instability of the breathing wave train associated to the spiral. In addition, the destabilization process may be influenced by the phase of the breathing oscillation which changes along the spiral arm. More detailed numerical investigation are needed to shed light on the precise mechanism.

Another difference from the above-cited examples is that in our case the final pattern observed is not chaotic spiral turbulence, but a spatially-complex and time-periodic multi-core pattern. We believe that even in FitzHugh-Nagumo-like systems, by choosing initial conditions seeded with additional spiral cores and setting the parameters so that no planar instability occurs, the appearance of a qualitatively similar pattern is possible. Indeed, this has been reported in [19, p. 125] for a system of forced coupled oscillators. However, we remark that in our case such complex pattern can be generated from a very simple one-core initial condition thanks to spiral breakup, which limits the size a single spiral can achieve.

As r_3 is reduced, the breakup starts to occur nearer to the spiral core. As a consequence, the central spiral grows less before destabilizing and the number of new spiral cores increases. The pattern still behaves periodically in the long run, but the initial transient phase is longer. Moreover, it becomes possible that the initial spiral is no longer included in the final pattern and disappears by interaction with the nearby spiral cores, as can be seen in Figure 23 for $r_3 = 26.8$. It should be noted that, although $r_3 = 26.8$ already lies inside the parameter region for which reflection occurs in one spatial dimension, due to the effect of curvature many front interactions do not result in complete reflection, but display breathing behaviour.

A further reduction of the parameter r_3 results in the central main spiral no longer being formed. New spiral cores are still generated by the incomplete reflection mechanism, although

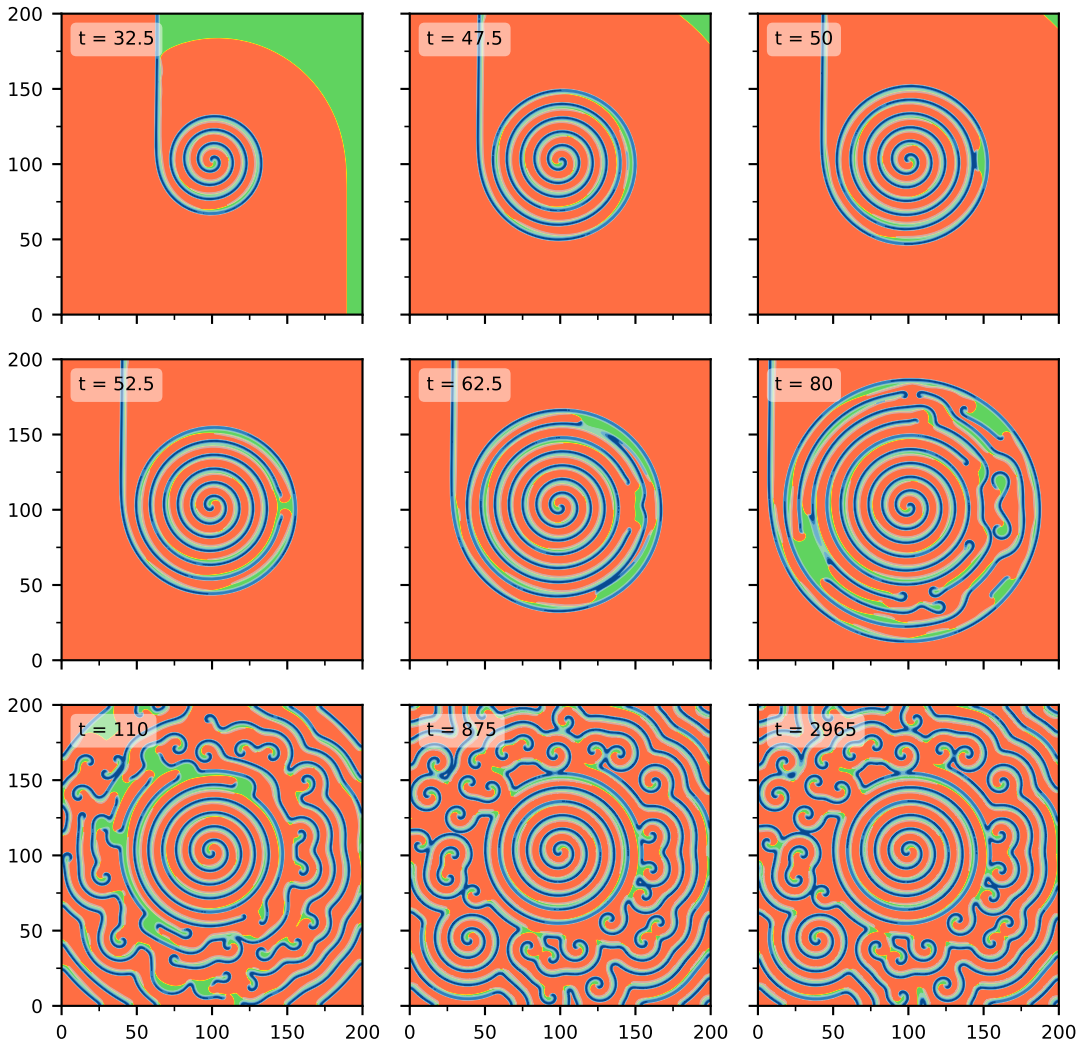


Figure 22 In the case $r_3 = 26.8175$, initial conditions as in Figure 19 (left panel) lead to a complex periodic pattern characterized by many spiral cores.

no spiral grows around them, as can be seen in Figure 24 (panels 1–4) for $r_3 = 26.75$. Since front interactions result in the complete reflection of fronts more often than before, no spiral core is able to survive for a long time. Old cores are continuously destroyed and new ones generated, leading to a very complex spatio-temporal pattern which is no longer periodic but chaotic in appearance, as can be seen in Figure 24 (panels 5–6). This is the same type of pattern we observed in Figure 2 at the beginning of this paper.

8 Concluding remarks

In this paper we studied the invasion by an exotic species w of an ecosystem inhabited by two native species u and v. The invader was supposed to be relatively weak compared to the native species, since it evolved in a different environment. By using a three-species competition-diffusion

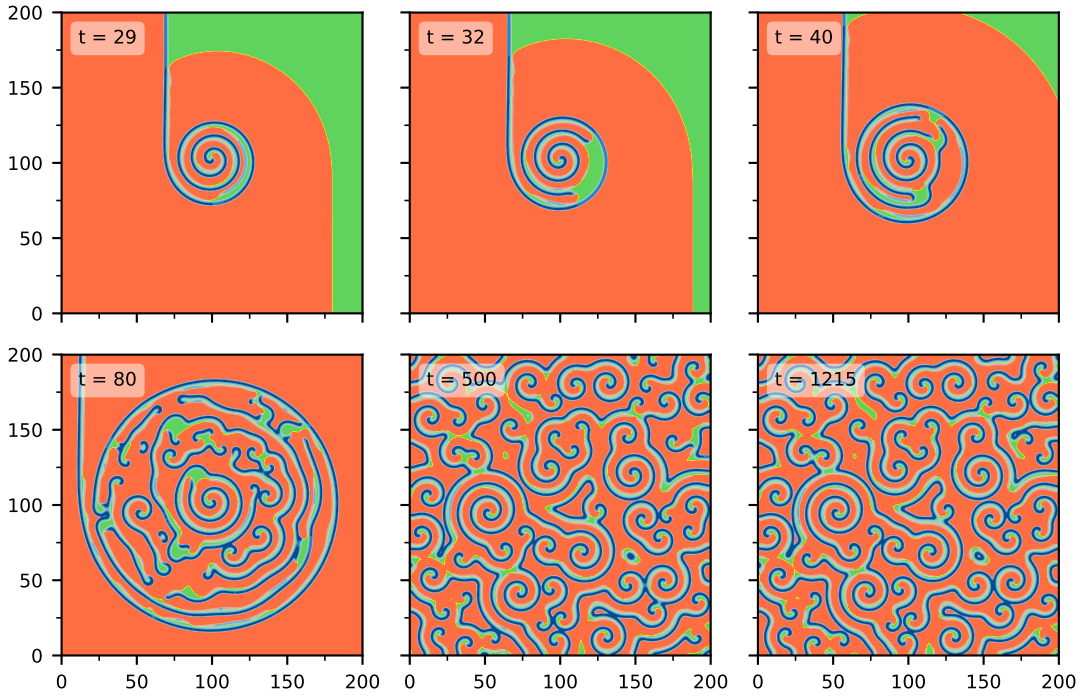


Figure 23 In the case $r_3 = 26.8$, initial conditions as in Figure 19 (left panel) lead to a complex periodic pattern characterized by many spiral cores, as it was the case in Figure 22. However, the initial spiral no longer survives in the long run.

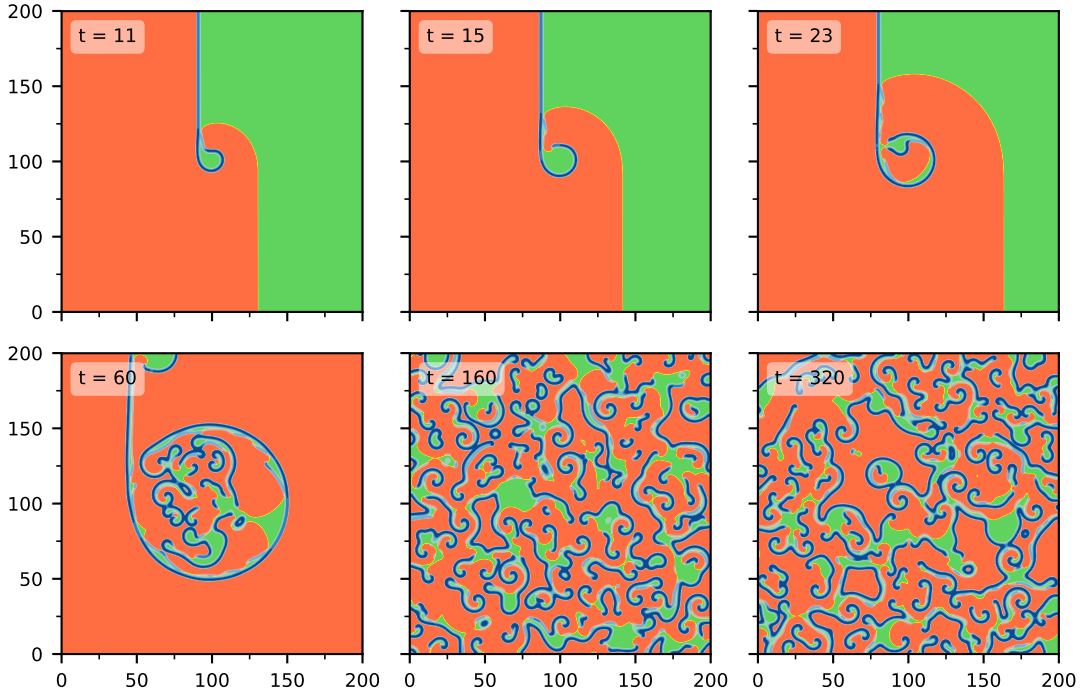


Figure 24 In the case $r_3 = 26.75$, initial conditions as in Figure 19 (left panel) lead to a complex non-periodic pattern characterized by the continuous birth and destruction of small spiral cores.

system and taking r_3, the intrinsic growth rate of w, as a free parameter, we investigated whether competitive exclusion or competitor-mediated coexistence occurs. Sensitively depending on the value of r_3, we found that in two spatial dimensions the system generates very complex spatio-temporal patterns which allow the three species to coexist dynamically.

The main purpose of this paper was to reveal the mechanism behind the occurrence of such complex patterns. From a visual inspection of the simulation results, it is clear that the patterns are generated by the interaction of two different kinds of moving fronts. For this reason, we started by studying the one-dimensional travelling waves of the system, finding that for intermediate values of r_3 there exist two types of stable waves. When their interaction is considered, depending on their relative velocity Δc different outcomes can be observed. If Δc is small in modulus, the two waves merge into a single travelling pulse. As Δc becomes larger, this pulse is destabilized through Hopf bifurcation and a travelling pulse whose width oscillates (breathing wave) can be observed. Then, colliding waves still merge, but become a breathing wave instead. Finally, when Δc is quite large the breathing wave no longer exists and colliding waves are reflected.

After that, we considered the two-dimensional case again, studying the interaction of the planar extensions of the two stable travelling waves, which for equal diffusion coefficients are also stable. Using the insight obtained from the one-dimensional case, we were able to see more clearly that a similar transition occurs in two spatial dimensions, explaining the onset of the complex patterns we observed. First, for Δc small in modulus, a regular and stable spiral exists in association to the one-dimensional stable pulse. As Δc becomes larger, the pulse width starts to oscillate: the regular spiral becomes unstable, but we still have a stable breathing spiral whose arm width oscillates. A further increase of Δc leads to larger oscillations which eventually cause the spiral to break up, generating additional spiral cores. The resulting pattern appears to be periodic, with the maximum possible spiral size decreasing as Δc becomes larger. At a certain point, reflection of fronts becomes more common than oscillating behaviour. As a consequence, the spiral cores are no longer persistent, but are dynamically destroyed and generated, resulting in an extremely complex non-periodic pattern.

The main ingredients for the appearance of the complex patterns are thus two, the existence of spiral cores and the reflection/breathing dynamics. The spiral cores allow the species to coexist locally, thus preventing competitive exclusion, which would result in the absence of any pattern. Reflection-like front interaction prevents the formation of spirals and eventually destroys the spiral cores, while breathing-like interaction leads to the formation of new spiral cores. Thanks to the effect of front curvature both reflection and breathing behaviour can coexist for a range of values of r_3, in which case we can observe a complex and chaotic pattern characterized by the dynamic generation and destruction of new spiral cores.

The same mechanism of spiral generation from a stable travelling pulse is observed in many FitzHugh-Nagumo-like reaction-diffusion systems. Additionally, in such systems spiral breakup and spiral turbulence are often observed when the pulse is no longer planarly stable [19, 35, 51], leading to patterns qualitatively similar to that in Figure 2. In particular, our system shares many similarities with the cases in which two stable Bloch fronts are generated from a nonequilibrium Ising-Bloch (NIB) bifurcation. These two Bloch fronts connect the same asymptotic states but travel in opposite directions, interact in complex ways and may exhibit breathing behaviour [33], making them very similar to the trivial and non-trivial fronts studied in this paper.

We conclude by summarizing what we believe are the most novel points introduced in this work.

- In the case of a system with a NIB bifurcation the interaction of two stable non-trivial (Bloch) fronts bifurcating from the same trivial (Ising) front is considered with similar results. However, in our case the interacting fronts are a stable non-trivial front and the stable trivial front, since the second non-trivial front is unstable. This is not the same as considering the imperfect pitchfork bifurcation obtained by perturbing the NIB (pitchfork) bifurcation [32], since the non-trivial front is still generated from the trivial front by a drift bifurcation. It may be possible to find a parameter set for which even in our case the drift bifurcation is a pitchfork (and thus a NIB) bifurcation, but in that case we expect one of the Bloch fronts to display negative density values for the species w and thus be non-admissible.

- We have shown how the existence of a breathing travelling pulse is very important in order to explain the outcome of pattern formation. In particular, the unstable breathing wave acts as a separator between reflection and merging dynamics, fulfilling a similar role to the scattors in the Gray-Scott model [60]. Finally, the bifurcation structure of the unstable branch as the period tends to infinity is quite interesting from a mathematical point of view and should be object of a deeper investigation.

- While the exact mechanism leading to spiral breakup will require further investigations to be precisely determined, we believe it to be linked to the destabilization of the time-periodic wave train associated to the breathing spiral. The varying phase of the breathing oscillation along the spiral arm may also be an influencing factor. Planar instability does not seem to play a role, since the trivial and non-trivial fronts, together with the travelling/breathing pulse, appear to be planarly stable when the diffusion coefficients of all three species are equal. This makes our case different from spiral breakup due to lateral instability, such as that reported in [35] and studied by singular perturbation in [37, 36].

- By the time spiral break-up occurs the regular spiral has already been destabilized by Hopf bifurcation, generating a stable breathing spiral. Such breathing pattern, except for the cases of forced systems [5, 28] or non-convex domains [63], is still not widely documented.

- For a given value of the free parameter r_3, the observed two-dimensional patterns are not completely determined by the one-dimensional travelling wave behaviour because curvature plays an important role. Higher front curvature promotes merging of the fronts, allowing both reflection and breathing dynamics to coexist, enlarging the range of parameters for which coexistence is possible compared to what could be expected by just considering the one-dimensional case. Moreover, this mechanism prevents any spiral to grow too large, allowing the generation of a periodic many-core pattern even in the presence of a very simple initial condition.

Acknowledgements

LC has been supported by the Meiji Institute for Advanced Study of Mathematical Sciences and by JSPS KAKENHI Grant-in-Aid for Research Activity Start-up JP16H07254. MM has been partially supported by JSPS KAKENHI Grant No. 15K13462.

References

[1] *1,4-Cyclohexanedione Belousov-Zhabotinsky Reaction*. Accessed: 2017-09-29. 2016. URL: https://www.youtube.com/watch?v=8tArShb1fhw.

[2] M. W. Adamson and A. Y. Morozov. "Revising the Role of Species Mobility in Maintaining Biodiversity in Communities with Cyclic Competition". In: *Bulletin of Mathematical Biology* 74.9 (2012), pp. 2004–2031. DOI: 10.1007/s11538-012-9743-z.

[3] M. Bär and L. Brusch. "Breakup of spiral waves caused by radial dynamics: Eckhaus and finite wavenumber instabilities". In: *New Journal of Physics* 6 (2004), p. 5. DOI: 10.1088/1367-2630/6/1/005.

[4] I. V. Barashenkov and S. R. Woodford. "Complexes of stationary domain walls in the resonantly forced Ginsburg-Landau equation". In: *Physical Review E* 71 (2 2005), p. 026613. DOI: 10.1103/PhysRevE.71.026613.

[5] I. Berenstein, A. P. Muñuzuri, L. Yang, M. Dolnik, A. M. Zhabotinsky, and I. R. Epstein. "Breathing spiral waves in the chlorine dioxide-iodine-malonic acid reaction-diffusion system". In: *Physical Review E* 78 (2 2008), p. 025101. DOI: 10.1103/PhysRevE.78.025101.

[6] M. Bode. "Front-bifurcations in reaction-diffusion systems with inhomogeneous parameter distributions". In: *Physica D: Nonlinear Phenomena* 106.3 (1997), pp. 270–286. DOI: 10.1016/S0167-2789(97)00050-X.

[7] A. Cangiani, E. H. Georgoulis, A. Y. Morozov, and O. J. Sutton. "Revealing new dynamical patterns in a reaction-diffusion model with cyclic competition via a novel computational framework". In: *Proceedings of the Royal Society of London A* 474.2213 (2018). DOI: 10.1098/rspa.2017.0608.

[8] C.-C. Chen, L.-C. Hung, M. Mimura, M. Tohma, and D. Ueyama. "Semi-exact equilibrium solutions for three-species competition-diffusion systems". In: *Hiroshima Mathematical Journal* 43.2 (2013), pp. 179–206. URL: https://projecteuclid.org/euclid.hmj/1372180511.

[9] C.-C. Chen and L.-C. Hung. "A maximum principle for diffusive Lotka–Volterra systems of two competing species". In: *Journal of Differential Equations* 261.8 (2016), pp. 4573–4592. DOI: 10.1016/j.jde.2016.07.001.

[10] L. Contento, M. Mimura, and M. Tohma. "Two-dimensional traveling waves arising from planar front interaction in a three-species competition-diffusion system". In: *Japan Journal of Industrial and Applied Mathematics* 32.3 (2015), pp. 707–747. DOI: 10.1007/s13160-015-0186-4.

[11] L. Contento, D. Hilhorst, and M. Mimura. "Ecological invasion in competition-diffusion systems when the exotic species is either very strong or very weak". In: *Journal of Mathematical Biology* 77.5 (2018), pp. 1383–1405. DOI: 10.1007/s00285-018-1256-4.

[12] L. Contento and M. Mimura. *Breathing travelling wave solutions in a three-species competition-diffusion system*. 2018. DOI: 10.5281/zenodo.1208443.

[13] L. Contento and M. Mimura. *Interaction of one-dimensional trivial and non-trivial travelling waves in a three-species competition-diffusion system*. 2018. DOI: 10.5281/zenodo.1208426.

[14] L. Contento and M. Mimura. *Interaction of planarly stable trivial and non-trivial travelling waves in a three-species competition-diffusion system*. 2018. DOI: 10.5281/zenodo.1208408.

[15] L. Contento and M. Mimura. *Invasion by an exotic species in a three-species competition-diffusion system*. 2018. DOI: 10.5281/zenodo.1208439.

[16] L. Contento and M. Mimura. *Perturbing the travelling pulse in a three-species competition-diffusion system*. 2018. DOI: 10.5281/zenodo.1208454.

[17] E. Conway, D. Hoff, and J. Smoller. "Large Time Behavior of Solutions of Systems of Nonlinear Reaction-Diffusion Equations". In: *SIAM Journal on Applied Mathematics* 35.1 (1976), pp. 1–16. DOI: 10.1137/0135001.

[18] P. Coullet, J. Lega, B. Houchmandzadeh, and J. Lajzerowicz. "Breaking chirality in nonequilibrium systems". In: *Physical Review Letters* 65 (11 1990), pp. 1352–1355. DOI: 10.1103/PhysRevLett.65.1352.

[19] P. Coullet and K. Emilsson. "Strong resonances of spatially distributed oscillators: a laboratory to study patterns and defects". In: *Physica D: Nonlinear Phenomena* 61.1 (1992), pp. 119–131. DOI: 10.1016/0167-2789(92)90154-F.

[20] E. J. Doedel, B. E. Oldeman, A. R. Champneys, F. Dercole, T. F. Fairgrieve, Y. Kuznetsov, R. C. Paffenroth, B. Sandstede, X. J. Wang, and C. H. Zhang. *AUTO-07p: Continuation and bifurcation software for ordinary differential equations*. 2012. URL: http://sourceforge.net/projects/auto-07p/.

[21] S.-I. Ei, H. Ikeda, M. Mimura, and T. Ogawa. "Drift bifurcation of traveling wave in reaction-diffusion system with 3 competing species". Joint Australia-Japan Workshop on dynamical systems with applications in life sciences. July 2016. URL: https://sites.google.com/site/petervanheijster/workshop/abstracts#OGAWA_ABSTRACT.

[22] S.-I. Ei, R. Ikota, and M. Mimura. "Segregating partition problem in competition-diffusion systems". In: *Interfaces and Free Boundaries* 1.1 (1999), pp. 57–80. DOI: 10.4171/IFB/4.

[23] C. Elphick, A. Hagberg, B. Malomed, and E. Meron. "On the origin of traveling pulses in bistable systems". In: *Physics Letters A* 230.1 (1997), pp. 33–37. DOI: 10.1016/S0375-9601(97)00228-4.

[24] C. Elphick, A. Hagberg, and E. Meron. "Dynamic front transitions and spiral-vortex nucleation". In: *Physical Review E* 51 (4 1995), pp. 3052–3058. DOI: 10.1103/PhysRevE.51.3052.

[25] A. Esteban-Martín, V. B. Taranenko, J. García, G. J. de Valcárcel, and E. Roldán. "Controlled Observation of a Nonequilibrium Ising-Bloch Transition in a Nonlinear Optical Cavity". In: *Physical Review Letters* 94 (22 2005), p. 223903. DOI: 10.1103/PhysRevLett.94.223903.

[26] T. Frisch. "Spiral waves in nematic and cholesteric liquid crystals". In: *Physica D: Nonlinear Phenomena* 84.3 (1995), pp. 601–614. DOI: 10.1016/0167-2789(94)00209-9.

[27] G. F. Gause. *The struggle for existence*. The Williams & Wilkins Company, Baltimore, 1934.

[28] P. Ghosh and D. S. Ray. "Amplitude equations for breathing spiral waves in a forced reaction-diffusion system". In: *The Journal of Chemical Physics* 135.10 (2011), p. 104112. DOI: 10.1063/1.3632992.

[29] R. Goh and A. Scheel. "Pattern formation in the wake of triggered pushed fronts". In: *Nonlinearity* 29.8 (2016), p. 2196. DOI: 10.1088/0951-7715/29/8/2196.

[30] D. Gomila, P. Colet, and D. Walgraef. "Theory for the Spatiotemporal Dynamics of Domain Walls close to a Nonequilibrium Ising-Bloch Transition". In: *Physical Review Letters* 114 (8 2015), p. 084101. DOI: 10.1103/PhysRevLett.114.084101.

[31] S. V. Gurevich, H. U. Bodeker, A. S. Moskalenko, A. W. Liehr, and H.-G. Purwins. "Drift Bifurcation of Dissipative Solitons: Destabilisation Due to a Change of Shape". In: *Proceedings of the 2003 International Conference on Physics and Control.* Vol. 2. 2003, pp. 601–606. DOI: 10.1109/PHYCON.2003.1236901.

[32] A. Hagberg and E. Meron. "Complex patterns in reaction-diffusion systems: A tale of two front instabilities". In: *Chaos: An Interdisciplinary Journal of Nonlinear Science* 4.3 (1994), pp. 477–484. DOI: 10.1063/1.166047.

[33] A. Hagberg and E. Meron. "Pattern formation in non-gradient reaction-diffusion systems: the effects of front bifurcations". In: *Nonlinearity* 7.3 (1994), p. 805. DOI: 10.1088/0951-7715/7/3/006.

[34] A. Hagberg and E. Meron. "Domain walls in nonequilibrium systems and the emergence of persistent patterns". In: *Physical Review E* 48 (2 1993), pp. 705–708. DOI: 10.1103/PhysRevE.48.705.

[35] A. Hagberg and E. Meron. "From labyrinthine patterns to spiral turbulence". In: *Physical Review Letters* 72 (15 1994), pp. 2494–2497. DOI: 10.1103/PhysRevLett.72.2494.

[36] A. Hagberg and E. Meron. "Order parameter equations for front transitions: Nonuniformly curved fronts". In: *Physica D: Nonlinear Phenomena* 123.1 (1998), pp. 460–473. DOI: 10.1016/S0167-2789(98)00143-2.

[37] A. Hagberg and E. Meron. "The Dynamics of Curved Fronts: Beyond Geometry". In: *Physical Review Letters* 78 (6 1997), pp. 1166–1169. DOI: 10.1103/PhysRevLett.78.1166.

[38] D. Haim, G. Li, Q. Ouyang, W. D. McCormick, H. L. Swinney, A. Hagberg, and E. Meron. "Breathing Spots in a Reaction-Diffusion System". In: *Physical Review Letters* 77 (1 1996), pp. 190–193. DOI: 10.1103/PhysRevLett.77.190.

[39] M. W. Hirsch. *Differential equations and convergence almost everywhere of strongly monotone semiflows.* Tech. rep. University of California, Berkeley, 1982.

[40] J. Hofbauer and K. Sigmund. *Evolutionary games and population dynamics.* Cambridge University Press, 1998. ISBN: 9780521625708.

[41] G. E. Hutchinson. "The Paradox of the Plankton". In: *The American Naturalist* 95.882 (1961), pp. 137–145. DOI: 10.1086/282171.

[42] H. Ikeda. "Singular pulse wave bifurcations from front and back waves in bistable reaction-diffusion systems". In: *Methods and Applications of Analysis* 3.3 (1996), pp. 285–317. DOI: 10.4310/MAA.1996.v3.n3.a1.

[43] T. Ikeda, H. Ikeda, and M. Mimura. "Hopf bifurcation of travelling pulses in some bistable reaction-diffusion systems". In: *Methods and Applications of Analysis* 7.1 (2000), pp. 165–194. DOI: 10.4310/MAA.2000.v7.n1.a8.

[44] Y. Kan-On. "Fisher wave fronts for the Lotka-Volterra competition model with diffusion". In: *Nonlinear Analysis: Theory, Methods & Applications* 28.1 (1997), pp. 145–164. DOI: 10.1016/0362-546X(95)00142-I.

[45] Y. Kan-On. "Parameter dependence of propagation speed of travelling waves for competition-diffusion equations". In: *SIAM Journal on Mathematical Analysis* 26.2 (1995), pp. 340–363. DOI: 10.1137/S0036141093244556.

[46] Y. Kan-On and Q. Fang. "Stability of monotone travelling waves for competition-diffusion equations". In: *Japan Journal of Industrial and Applied Mathematics* 13.2 (1996), pp. 343–349. DOI: 10.1007/BF03167252.

[47] K. Kishimoto and H. F. Weinberger. "The spatial homogeneity of stable equilibria of some reaction-diffusion systems on convex domains". In: *Journal of Differential Equations* 58.1 (1985), pp. 15–21. DOI: 10.1016/0022-0396(85)90020-8.

[48] H. Kokubo. "Homoclinic and heteroclinic bifurcations of vector fields". In: *Japan Journal of Applied Mathematics* 5.3 (1988), pp. 455–501. DOI: 10.1007/BF03167912.

[49] H. Kokubu, Y. Nishiura, and H. Oka. "Heteroclinic and homoclinic bifurcations in bistable reaction diffusion systems". In: *Journal of Differential Equations* 86.2 (1990), pp. 260–341. DOI: 10.1016/0022-0396(90)90033-L.

[50] K. J. Lee and H. L. Swinney. "Lamellar structures and self-replicating spots in a reaction-diffusion system". In: *Physical Review E* 51.3 (1995), pp. 1899–1915. DOI: 10.1103/PhysRevE.51.1899.

[51] A. F. M. Marée and A. V. Panfilov. "Spiral Breakup in Excitable Tissue due to Lateral Instability". In: *Physical Review Letters* 78 (9 1997), pp. 1819–1822. DOI: 10.1103/PhysRevLett.78.1819.

[52] B. Marts, A. Hagberg, E. Meron, and A. L. Lin. "Bloch-Front Turbulence in a Periodically Forced Belousov-Zhabotinsky Reaction". In: *Physical Review Letters* 93 (10 2004), p. 108305. DOI: 10.1103/PhysRevLett.93.108305.

[53] H. Matano and M. Mimura. "Pattern Formation in Competition-Diffusion Systems in Nonconvex Domains". In: *Publications of the Research Institute for Mathematical Sciences* 19.3 (1983), pp. 1049–1079. DOI: 10.2977/prims/1195182020.

[54] K. B. Migler and R. B. Meyer. "Spirals in liquid crystals in a rotating magnetic field". In: *Physica D: Nonlinear Phenomena* 71.4 (1994), pp. 412–420. DOI: 10.1016/0167-2789(94)90007-8.

[55] M. Mimura and M. Nagayama. "Nonannihilation dynamics in an exothermic reaction-diffusion system with mono-stable excitability". In: *Chaos: An Interdisciplinary Journal of Nonlinear Science* 7.4 (1997), pp. 817–11. DOI: 10.1063/1.166282.

[56] M. Mimura and M. Tohma. "Dynamic coexistence in a three-species competition-diffusion system". In: *Ecological Complexity* 21 (2015), pp. 215–232. DOI: 10.1016/j.ecocom.2014.05.004.

[57] Y. Morita and K. Tachibana. "An Entire Solution to the Lotka-Volterra Competition-Diffusion Equations". In: *SIAM Journal on Mathematical Analysis* 40.6 (2009), pp. 2217–2240. DOI: 10.1137/080723715.

[58] J. D. Murray. *Mathematical biology: I. An Introduction*. Springer, 2002. ISBN: 978-0-387-95223-9. DOI: 10.1007/b98868.

[59] M. Nagayama, K. Ueda, and M. Yadome. "Numerical approach to transient dynamics of oscillatory pulses in a bistable reaction–diffusion system". In: *Japan Journal of Industrial and Applied Mathematics* 27.2 (2010), pp. 295–322. DOI: 10.1007/s13160-010-0015-8.

[60] Y. Nishiura, T. Teramoto, and K. Ueda. "Scattering and separators in dissipative systems". In: *Physical Review E* 67.5 (2003), p. 056210. DOI: 10.1103/PhysRevE.67.056210.

[61] I. Pérez-Arjona, F. Silva, G. J. de Valcárcel, E. Roldán, and V. J. Sánchez-Morcillo. "The Ising-Bloch transition in degenerate optical parametric oscillators". In: *Journal of Optics B: Quantum and Semiclassical Optics* 6.5 (2004), S361. DOI: 10.1088/1464-4266/6/5/026.

[62] W. N. Reynolds, J. E. Pearson, and S. Ponce-Dawson. "Dynamics of self-replicating patterns in reaction diffusion systems". In: *Physical Review Letters* 72.17 (1994), p. 2797. DOI: 10.1103/PhysRevLett.72.2797.

[63] H. Sakaguchi and Y. Nakamura. "Elimination of Breathing Spiral Waves in the Aliev-Panfilov Model". In: *Journal of the Physical Society of Japan* 79.7 (2010), p. 074802. DOI: 10.1143/JPSJ.79.074802.

[64] V. J. Sánchez-Morcillo, V. Espinosa, I. Pérez-Arjona, F. Silva, G. J. de Valcárcel, and E. Roldán. "Domain wall dynamics in an optical Kerr cavity". In: *Physical Review E* 71 (6 2005), p. 066209. DOI: 10.1103/PhysRevE.71.066209.

[65] B. Sandstede and A. Scheel. "Gluing unstable fronts and backs together can produce stable pulses". In: *Nonlinearity* 13.5 (2000), p. 1465. DOI: 10.1088/0951-7715/13/5/303.

[66] J. Yang, F. Xie, Z. Qu, and A. Garfinkel. "Mechanism for Spiral Wave Breakup in Excitable and Oscillatory Media". In: *Physical Review Letters* 91.14 (2003), p. 148302. DOI: 10.1103/PhysRevLett.91.148302.

[67] M. L. Zeeman. "Hopf bifurcations in competitive three-dimensional Lotka-Volterra systems". In: *Dynamics and Stability of Systems* 8.3 (1993), pp. 189–216. DOI: 10.1080/02681119308806158.

[68] Y. R. Zelnik and E. Meron. "Regime shifts by front dynamics". In: *Ecological Indicators* 94 (2018), pp. 544–552. DOI: 10.1016/j.ecolind.2017.10.068.

[69] L. Q. Zhou and Q. Ouyang. "Spiral Instabilities in a Reaction-Diffusion System". In: *The Journal of Physical Chemistry A* 105.1 (2001), pp. 112–118. DOI: 10.1021/jp002430h.